Ocean Modelling xxx (2008) xxx–xxx

Contents lists available at ScienceDirect

Ocean Modelling

journal homepage: www.elsevier.com/locate/ocemod

The mesoscale variability in the Caribbean Sea. Part I: Simulations and characteristics with an embedded model

Julien Jouanno [a,*], Julio Sheinbaum [a], Bernard Barnier [b], Jean-Marc Molines [b], Laurent Debreu [c], Florian Lemarié [c]

[a] Departamento de Oceanografia Física, CICESE, Km. 107 Carretera Tijuana-Ensenada, Ensenada, C.P. 22860, Baja California, Mexico
[b] MEOM, LEGI-CNRS, BP53, 38041, Grenoble Cedex 9, France
[c] Institut d'Informatique et de Mathématiques Appliquées de Grenoble, Laboratoire de Modélisation et Calcul, BP 53, 38041, Grenoble, Cedex 9, France

ARTICLE INFO

Article history:
Received 1 January 2008
Received in revised form 20 March 2008
Accepted 3 April 2008
Available online xxxx

Keywords:
Caribbean
Ocean model
Embedding
Mesoscale eddies
Instability

ABSTRACT

The variability in the Caribbean Sea is investigated using high resolution (1/15°) general circulation model experiments. For the first time in this region, simulations were carried out with a 2-way nested configuration of the NEMO primitive equation model. A coarse North Atlantic grid (1/3°) reproduces the main features of the North Atlantic and Equatorial circulation capable of influencing ocean dynamics in the Caribbean Sea. This numerical study highlights strong dynamical differences among basins and modifies the view that dynamics are homogeneous over the whole Caribbean Basin. The Caribbean mean flow is shown to organize in two intense jets flowing westward along the northern and southern boundaries of the Venezuela Basin, which merge in the center of the Colombia Basin. Diagnostics of model outputs show that width, depth and strength of baroclinic eddies increase westward from the Lesser Antilles to the Colombia Basin. The widening and strengthening to the west is consistent with altimetry data and drifter observations. Although influenced by the circulation in the Colombia Basin, the variability in the Cayman Basin (which also presents a westward growth from the Chibcha Channel) is deeper and less energetic than the variability in the Colombia/Venezuela Basins. Main frequency peaks for the mesoscale variability present a westward shift, from roughly 50 days near the Lesser Antilles to 100 days in the Cayman Basin, which is associated with growth and merging of eddies.

1. Introduction

The existence of a strong mesoscale activity in the Caribbean Sea is receiving increasing attention. First, the generation of large and energetic eddies poses very interesting dynamical questions. Second, the local and global implications of this mesoscale activity still have to be determined. For example the process whereby the Loop Current sheds anticyclones in the Gulf of Mexico is not well understood but has been shown to be related to the flux of potential vorticity (PV) through the Yucatan Channel (Candela et al., 2003). This PV flux is apparently driven by the variability in the Caribbean Sea. Another example is the trapping of larvae by the eddies and their advection over large distances (Group, 1981). Mesoscale anticyclones are also though to contribute significantly to the meridional overturning circulation (Johns et al., 2002), transporting southern hemisphere waters to the north. The circulation in the Caribbean Sea is also part of the North Atlantic Subtropical Gyre (e.g., Schmitz and McCartney, 1993). Interesting questions arise regarding the effect that local processes may have on these large-scale circulation systems or, in the opposite sense, the role that variations at the basin scale play in determining the variability within the Caribbean.

In situ observations in the Caribbean Sea are scarce and mainly limited to coastal regions and passages between the numerous islands (e.g., Johns et al., 2002). We can mention the meridional hydrographic section from Venezuela to Puerto Rico of Hernández-Guerra and Joyce (2000). It provides valuable information about current and hydrographic structure of the region, but this is only one realization which is not necessarily representative of the mean conditions in the region. Most of the characteristics of the eddies in the Caribbean interior have to be inferred by altimetry, which to date is the only source of long term surface observations. Ten years of sea level anomalies from altimetry data show that the whole Caribbean supports a strong anticyclonic and cyclonic eddy activity in the upper layers (Guerrero et al., in press). The observed events have periods from 50 to 100 days, diameters from 200 to 500 km and travel westward with a mean speed between 0.12 and 0.15 m s^{-1}. In this study, a predominance of anticyclones often suggested by numerical models has been shown. A previous study with 15 months of altimetry data (Andrade and Barton, 2000), also revealed large and energetic anticyclones and cyclones,

* Corresponding author. Tel.: +52 (646) 2850500.
E-mail address: jouanno@cicese.mx (J. Jouanno).

1463-5003/$ - see front matter © 2008 Elsevier Ltd. All rights reserved.
doi:10.1016/j.ocemod.2008.04.002

advected at 20 cm s^{-1}. They remarked the formation of eddies embedded in the Colombia–Panama Gyre in the southern Colombia Basin. Using in situ data, Silander (2005) studied an anticyclone, a cyclone and an eddy pair in the Venezuela basin. They found maximum swirl speeds of 0.3–0.6 m s^{-1} and westward propagation speeds ranging from 0.06 to 0.12 m s^{-1}. L-ADCP (lowered acoustic Doppler current profiler) data showed a coherent vertical structure down to 1000 m depth and possibly more. During the tracking, they observed strengthening and merging of the eddies. Analyzing two years of drifter data, Richardson (2005) found the Venezuela and Colombia Basins (see Fig. 1) were dominated by energetic anticyclones, with a typical swirl speed of 0.6 m s^{-1} and diameters near 200 km, traveling west to the Central America Rise, where he suggests that the eddies are disrupted by topography. He estimates a production of 8–12 eddies per year with a maximum from September to November and a minimum from February to May. His analysis shows that cyclones are preferably located near the South American coast of the Colombia and Venezuela basins. In the same study, he found that the translation velocity of the anticyclones depends on their route: embedded in strong jets they travel at 0.13 ms^{-1} but outside they travel slower. For example south of Cuba, two tracked anticyclones traveled westward at 0.02 ms^{-1}.

Many modeling studies have been carried out (e.g., Murphy et al., 1999; Carton and Chao, 1999; Oey et al., 2003) to understand the dynamics of the Caribbean Sea. Several features are recurrent in these simulations: predominance of anticyclones, westward intensification, dissipation near the coast of Nicaragua, horizontal length scales of 100–700 km, westward propagation speeds from 0.12 to 0.15 ms^{-1}. All those characteristics are robust features which seem independent of the forcing, model type (geopotential, isopycnal or sigma coordinates) and resolution if eddies are resolved. Nevertheless, the vertical extent of the eddies remains model dependent and often underestimated. Some experiments suggest that the eddies are mostly limited to the thermocline (e.g., Carton and Chao, 1999) but recent simulations with the σ-coordinates model ROMS produce eddies which reach 1000 m depth (Julio Sheinbaum, personal communication). Such deep vertical extent appears more consistent with the observations of Silander (2005), commented before, since L-ADCP data in the Venezuela Basin have shown cyclones and anticyclones with a coherent vertical structure down to 1000 m depth or more.

In this study, the characteristics of the mesoscale Caribbean eddy field are explored. We use the model NEMO, the new version of the former OPA model (Madec et al., 1998) in 2-way nested configurations. The nesting is managed by the AGRIF package. Circulation in the Caribbean Sea and the Gulf of Mexico are simulated with a grid of 1/15°. At this resolution, mesoscale dynamics and in particular instability processes are well resolved. A North Atlantic grid (1/3°) reproduces suitably the basic features of the North Atlantic circulation (between 20°S and 70°N) which can interact with the Caribbean dynamics: North Brazil Current (NBC) rings, Atlantic Rossby Waves, North Atlantic Subtropical Gyre, and Meridional Overturning Circulation (MOC). The following section presents with further details the model configuration and the various experiments which have been carried out. Section 3 describes the model mean flow and Section 4 the simulated eddy field and its characteristics. Results are compared with observations, when available. In both sections, the sensibility of simulated Caribbean circulation to model resolution and configuration is analyzed by comparing diagnostics (e.g., mean paths, eddy kinetic energy) from various numerical simulations. Finally, Section 5 gives a summary and conclusions.

2. Model configuration

2.1. Overview

In the introduction it was mentioned that circulation in the Gulf of Mexico and Caribbean Sea interacts with large scale circulation patterns such as the MOC, the Subtropical Gyre or with vorticity anomalies related to NBC rings. A correct representation of large scale patterns and their seasonal variations can be achieved with large scale model configurations, but for resolution of smaller scale

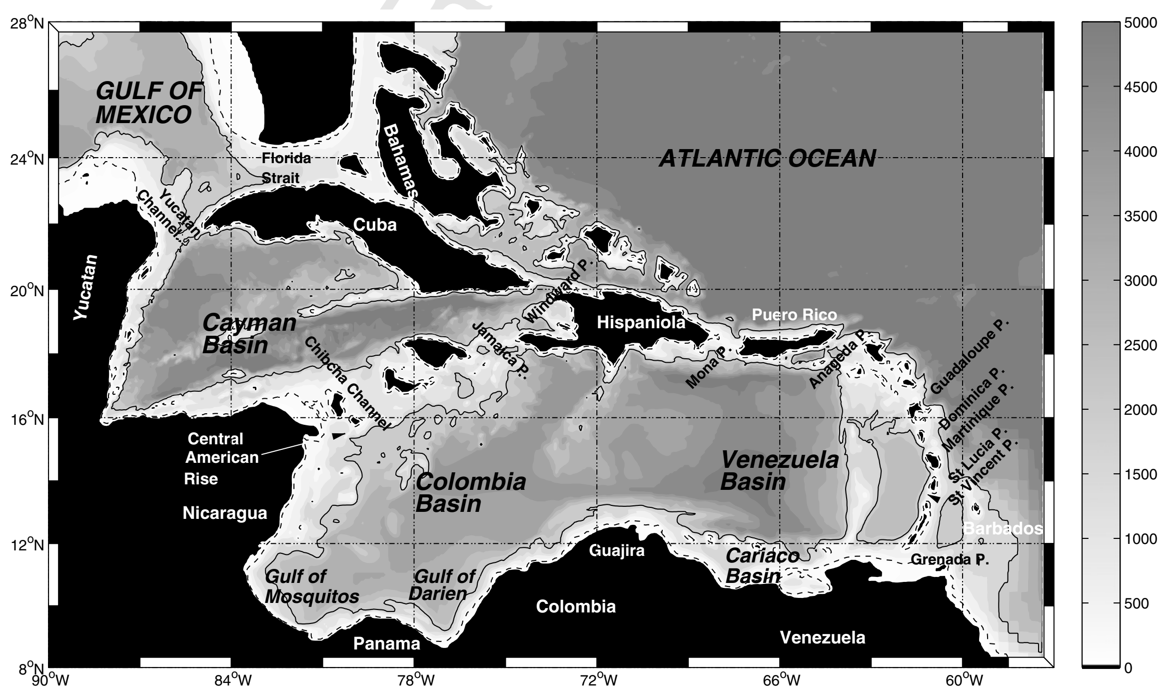

Fig. 1. Map and bathymetry of the Caribbean Sea and Gulf of Mexico. The dashed and full lines indicate respectively the 200 and 1000 m depth isobaths. "P." is the abbreviation of "Passage".

processes, an adequate representation of the Antilles Passages and an appropriate resolution of baroclinic instability processes requires the use of a sufficiently fine grid in the Caribbean region. High resolution simulations of the Atlantic basin circulation, such as CLIPPER-ATL6 (1/6°) and MERCATOR-PAM (1/12°), have already been used to study the Gulf of Mexico and the Caribbean Sea (Candela et al., 2003; Tanahara, 2004). But the computational cost of such simulations is particularly high to run series of diagnostic experiments. Because our study focuses specifically on the dynamics of the Caribbean Sea, we have chosen an embedded configuration, as illustrated in Fig. 2: a realistic, fine grid eddy-resolving (1/15°, ~7 km resolution) configuration of the Caribbean Sea and Gulf of Mexico (CAR15) is embedded in a coarser grid eddy-permitting North Atlantic 1/3° (~35 km) configuration (NATL3). Since our configuration involves only two grids, we will also refer to the coarse grid (NATL3) as the parent grid and the fine grid (CAR15) as the child grid. The numerical code used is the ocean general circulation model NEMO. It solves the three dimensional primitive equations in spherical coordinates discretized on a C-grid and fixed vertical levels (*z*-coordinate).

2.2. Grid refinement with AGRIF

The nesting is allowed by the AGRIF package (Debreu, 2000; Blayo and Debreu, 1999), a set of routines written in Fortran 90 which allows adaptive mesh refinement in a multidimensional model. AGRIF is able to deal with adaptive grids (see Debreu et al. (2005) for an adaptive application) but until now it has been mostly used in realistic simulations with fixed fine grids, as in the study of mesoscale eddies in the Labrador Sea (Chanut, 2003; Chanut et al., in press). Some illuminating details about the implementation of an AGRIF configuration can be found in Cailleau (2004) and Cailleau et al. (accepted for publication).

This method allows a recursive embedment of grids. Grids can be located on a same level or successively embedded without limit. So far, only horizontal refinement is available but new developments should allow vertical refinement in the future. Numerical schemes, parametrization and parameters of the different grids can be chosen independently. The ratio of spatial refinement can be even or uneven, but it is strongly recommended to be less or equal to 5. One should also keep in mind that configurations with too different horizontal resolutions may resolve very different physics, producing unrealistic dynamics at the boundary between grids.

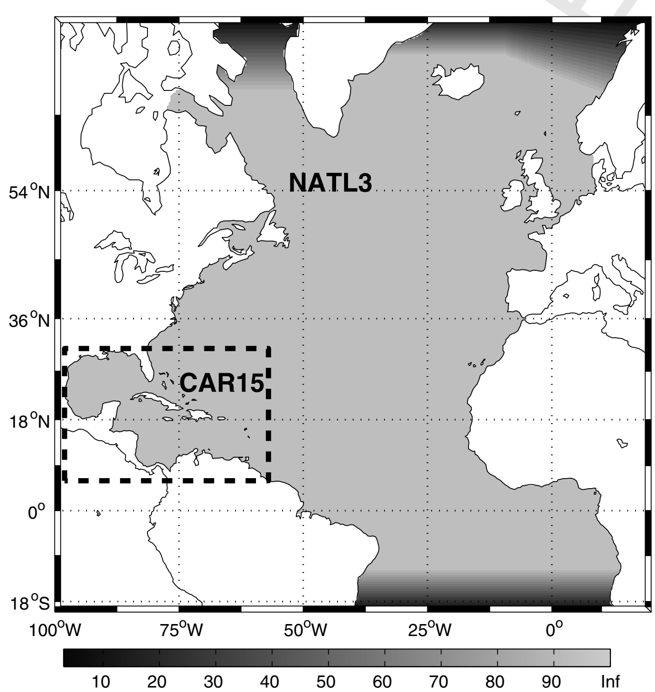

Fig. 2. Domains for the North Atlantic (1/3°) grid (NATL3) and the Caribbean Sea – Gulf of Mexico (1/15°) grid (CAR15, dashed rectangle). Shaded areas show the location of the buffer zones, the gray scale indicating the time scale (days) for the relaxation of the model variable toward a climatological reference.

AGRIF was designed to be easily adapted to already existing GCM codes. The basic strategy of the method consists in the use of "pointers". They allow to represent fields in different grids using the same set of computational arrays of variables. The procedure of integration is done recursively in the different grids, as described in Penven et al. (2006) for a 2 level embedding in a 1-way configuration. Here, we complete this procedure for a 2-way configuration taking the following steps:

(1) Advance the parent grid by one parent time step.
(2) Interpolate the relevant parent variables in space and time to get the boundary conditions for the child grid.
(3) Advance the child grid by as many child time steps as necessary to reach the new parent model time.
(4) Update the parent grid

In particular for the 4th step: 2D variables (e.g., sea surface height; SSH), which are used by the elliptic solver for the pressure, are updated for each time step on the whole region covered by the child grid, but 3D variables are updated at each time step only at few grid points at the boundary and its vicinity, and each five time steps on the rest of the domain. Two reasons justify this method. First, it preserves an efficient parallelization. Second, if the 3D variables were updated at each time step over the whole child grid region, problems would arise from the differences in volume between parent and child grids. At the boundary such problems are avoided by connecting the child bathymetry to the parent bathymetry. The connection is made on three coarse grid cells at the boundaries with the child grid.

Differences of resolution between grids imply an abrupt change of viscosity at the boundaries. During the integration, smoothing is applied at the boundary over a zone equivalent to two parent grid cells. Such smoothing is necessary to avoid numerical instabilities and to allow continuity of the physics between grids. An abrupt change could destroy patterns which enter the fine grid (e.g., NBC rings, Rossby Waves). It also prevents small scale patterns from reaching the coarse grid. In practice, the smoothing is applied to the difference between the two grid values and not directly on the fields from each grid, allowing diffusion to smooth the difference between small and large scales. This method reduces the transition effects on the momentum flux as well as the risk of making the boundary between grids become a physical boundary which could prevent or slow down the flow. Interpolations at the boundary between two grids do not allow an exact conservation of tracer and momentum fluxes, but the resulting bias is so small that it cannot have an impact on the results discussed in the paper. In 2-way interacting grids, values of the parent grid are replaced by a weighted mean of the child grid points.

The implementation of an AGRIF configuration requires a set of data arrays containing coordinates, bathymetry, forcings and initial conditions for each grid. In NEMO, the preparation of these data is simplified by a set of Fortran routines called "Nesting Tools" [1] developed at the Laboratoire Jean Kuntzmann. This module allows to interpolate and smooth the bathymetry from a finer bathymetry as well as to interpolate forcing and restart fields from the parent grid to the child grid.

[1] http://ljk.imag.fr/membres/Florian.Lemarié/NEMO_AGRIF.

2.3. Coarse grid model NATL3

The NATL3 configuration used here is very similar to that described in detail in Chanut et al. (in press) who used it with a similar AGRIF-based grid refinement to study eddies in the Labrador Sea. The only difference is that we have updated the OPA numerical code used in Chanut et al. (in press) by its new version NEMO. Run alone, it reproduces the main features of the North Atlantic circulation susceptible of influencing ocean dynamics in the Caribbean Sea: NBC Rings, subtropical Rossby Waves, North Atlantic Subtropical Gyre, the Loop Current and Loop Current Eddies, etc. Seasonal variation of these patterns in the model are in phase with the observed one. For example, the retroflection of the NBC is stronger in fall, consistent with other models (Barnier et al., 2001) and with observations of Johns et al. (2003).

An isotropic Mercator grid is used. Equations are discretized on an Arakawa C-grid at fixed vertical levels (z-coordinates). In the vertical, the grid has 43 vertical levels whose spacing increases from 12 m at the surface to 250 m below 1500 m. Partial steps, a NEMO feature not present in OPA, allow the thickness of the bottom cells to vary and hence improve the representation of the bottom topography, which is based on the Smith and Sandwell (1997) database, corrected in some places. This partial steps feature has been shown to drastically improve the model solution in the North Atlantic and the global ocean (Barnier et al., 2006; Penduff et al., 2007). Horizontal diffusion and viscosity are parametrized as bi-harmonic operators. The vertical mixing coefficient is given by a turbulent kinetic energy second-order closure scheme (Blanke and Delecluse, 1993) and is enhanced to a large value ($K_{\max} = 10\ \mathrm{m}^2\ \mathrm{s}^{-1}$) in case of static instability. The Atlantic domain is limited by three open boundaries located (1) at 70°N, (2) in the Gulf of Cadiz at 8°W, and (3) between Africa and America at 20°S (see Fig. 2). They radiate perturbations outward and relax the model variables to a climatological reference. Details can be found in Tréguier et al. (2001). The atmospheric forcing used is a climatological annual cycle of wind stress, heat and freshwater fluxes based on the daily-mean fields obtained by averaging ERA15 (the first "European Center for Medium range Weather Forecasting" ECMWF re-analysis) between 1979 and 1993 (Garnier et al., 2001). It is applied following the formulation of Barnier (1998) using flux corrections to parametrize air-sea feedback on fluxes.

2.4. The fine grid: CAR15

CAR15 is the fine (child) grid (1/15°-horizontal resolution). Most of its characteristics are similar to those from NATL3. Forcing fields are obtained by an interpolation of the NATL3 forcings. Vertical coordinates, advection scheme and methods of parametrization do not differ from those of NATL3. Details are summarized in Table 1 for both NATL3 and CAR15 grids. The main differences between the two grids are: two different bathymetry databases were used and some dynamical and parametrization parameters have been adjusted.

Table 1
Characteristics of NATL3 and CAR15 grids

Grid	NATL3	CAR15
Position of the grid	20.0°S–70°N −97.6°W–24.5°E	6.0°N–30.9°N −97.6°W–57.4°W
Bathymetry	ETOPO2 Smith and Sandwell (1997)	GEBCO IOC and BODC (2003)
Horizontal resolution	1/3° ∼35 km	1/15° ∼7 km
Number of horizontal points	358×361	604×399
Number of vertical levels	43	43
Time step	30 mn	10 mn
Bilaplacian horizontal diffusivity	$-2.5 \times 10^{11}\ \mathrm{m}^4\ \mathrm{s}^{-1}$	$-4 \times 10^{9}\ \mathrm{m}^4\ \mathrm{s}^{-1}$

In CAR15, the bottom topography (Fig. 1) is based on GEBCO IOC and BODC (2003). We have made this choice since the representation of the topography near the Yucatan coast is better than in the Smith and Sandwell (1997) bathymetry. In particular, the depth of the passage between Cozumel and Yucatan is about 100 m deep in Smith and Sandwell (1997) whereas GEBCO shows depth values down to 400 m which have been confirmed during CANEK (Abascal et al., 2003) oceanographic cruises. We have filled (i.e, depth equal to 0 m) regions with very shallow topography, such as the whole Bahamas Archipelago or the Maracaibo Lagoon. The depth of the points located at the northern and eastern boundaries of CAR15 (which interact with NATL3) have been interpolated from 3 coarse grid points to match the coarse bathymetry. It is worth mentioning that otherwise both topographies are very similar.

Although the spatial scale factor between grids is 5, configurations were integrated with a temporal scale factor equal to 3, saving a great deal of computer time without affecting the dynamics. This means the high resolution grid is 5 times finer than the low resolution grid, but the high resolution time-step is only 3 times smaller than in the coarse grid. This was possible because of the low latitude of the CAR15 model.

2.5. Numerical experiments

The same strategy has been used for most of the simulations which have been run. The coarse grid simulation is started from rest with temperature and salinity fields taken from Reynaud et al. (1998) climatological analysis. It is then spun-up for 8 years with a climatological daily forcing (i.e., without interannual variability), built by averaging the daily values of ECMWF-ERA15 reanalysis fluxes over years 1979–1993 and than applying a low-pass 10 days running mean filter. Such spin-up is long enough to stabilize the location of major fronts, like the Gulf Stream, it also allows first baroclinic mode Rossby waves to cross the Atlantic Ocean and the Subtropical Gyre to stabilize. Then, the coarse and fine grids are run together, interacting in 2-way. One year is necessary to allow the fine grid solution to stabilize. The dynamical spin-up of the 2-grid system is thus achieved after those 9 years of calculation. The system is integrated for six additional years with the same forcing, and model output are saved as successive 5-day averages and used for diagnostics.

The reasonable computational cost of an AGRIF configuration (i.e., NATL3 interacting in 2-way with CAR15) has allowed to run different experiments. It requires about 120 wall clock hours on 21 processors Opteron Dual Core on "Catavinya" (CICESE cluster) to compute 1 year of simulation. The same configuration with 128 Power4 processors on a IBM SP4 at IDRIS (CNRS supercomputer center), last roughly 20 h for 1 year of simulation.

The characteristics of the different simulations which have been analyzed for this work are summarized in Table 2. Four simulations were carried out with AGRIF (REF, MEAN, NOSLIP, VISC) and two without AGRIF (COARSE, CLIPPER). Following are the details of each of them:

Experiment REF. It is used as a reference for comparison with the other simulations. It does not provide the most realistic results, but it is the first which was carried out. NATL3 and CAR15 grids, which interact in 2-way, are forced with daily climatological forcing, as previously described. Free slip horizontal boundary conditions are used in both grids. Each of the three other embedded experiments run for this study presents only one change with respect to REF: horizontal boundary condition (NOSLIP), forcing (MEAN) and addition of viscosity near the Antilles (VISC). By changing only one characteristic, the com-

Please cite this article in press as: Jouanno, J. et al., The mesoscale variability in the Caribbean Sea. Part I: Simulations ..., Ocean Modell. (2008), doi:10.1016/j.ocemod.2008.04.002

Table 2
Characteristics of the experiments

Name	Horiz. resol.	AGRIF	Forcings	Partial steps	Horiz. boundary condition	Special feature
REF	1/15°	√	Daily clim.	√	Free slip	
MEAN	1/15°	√	Annual mean	√	Free slip	
NOSLIP	1/15°	√	Daily clim.	√	No slip	
VISC	1/15°	√	Daily clim.	√	Free slip	Laplacian viscosity is added (see Fig. 3)
COARSE	1/3°		Daily clim.	√	Free slip	NATL3 grid is run without embedment
CLIPPER	1/6°		Daily		Free slip	High resolution GCM (Tréguier et al., 1999)

parison of the different simulations and the interpretation of the differences are easier and more robust.

Experiment MEAN. Both grids of this simulation are forced by the annual mean of the daily climatological forcings used in REF. It eliminates variations driven by the seasonal forcing and causes a reduction of the NBC rings production. It was carried out for the purpose of analyzing the effect of NBC rings and Atlantic perturbations on the Caribbean Sea eddy activity.

Experiment NOSLIP. This experiment uses no-slip sidewall boundary conditions, in the fine grid (CAR15) instead of free-slip conditions. This run appears to be the most realistic when comparing outputs with altimetry, in particular the behavior of the NBC rings near the Lesser Antilles is better represented. For these reasons, this run is used for comparison with observations and diagnostics here and in part II of this study (Jouanno et al., submitted).

Experiment VISC. An enhanced Laplacian horizontal viscosity for the dynamics is added in the region between the NBC retroflection and the Lesser Antilles (2°S–17°N and 60°W–50°W, see Fig. 3). This addition is made on both NATL3 and CAR15 grids. It results in the dissipation of NBC rings and Atlantic Rossby waves before they reach the Lesser Antilles: no more mesoscale perturbations enter the Caribbean Sea. This simulation was carried out for the purpose of completing our understanding of the effect of NBC rings and Atlantic perturbations on the Caribbean Sea eddy activity.

Experiment COARSE. The coarse configuration NATL3 is run alone (without grid refinement). It has been carried out for comparisons with AGRIF configurations and to estimate the difference in the dynamics between 1/3° and 1/15° simulations. It is also a validation of the large scale circulation produced by NATL3.

Experiment CLIPPER. Experiment CLIPPER is the unique experiment not run especially for this work, but during the "CLIPPER" experiment (Tréguier et al., 1999). The version 8.1 of the OPA code was used. A detailed description of the experiment might be found in Penduff et al. (2004). Some of the characteristics which contrast with the other simulations are: no grid refinement, full-step bottom topography, ENS momentum advection scheme (Sadoumy, 1975), daily interannual forcing and 1/6° resolution over the whole Atlantic. This configuration was already used in a study of the dynamics of the Gulf of Mexico and the Yucatan Channel (Candela et al., 2003; Tanahara, 2004), but for the years 1989–1993 (i.e., during the period where the forcing has no interannual variability). These authors have shown a good agreement between simulated data and observations in this region. There are also some discrepancies. The first one is that the simulated transport through the Yucatan Channel (~28 Sv) is higher than the one observed (~24 Sv) by Sheinbaum et al. (2002). The comparison of T–S diagrams from simulated data with data collected during the CANEK observing program in the Yucatan Channel shows there is a too strong mixing in the first 100 m which reduces the stratification in the upper layers (Tanahara, 2004). In the model the mixing in the deeper layers is also shown to be over-estimated. They associate these problems with the discretization in z-coordinates and the relatively high numerical horizontal viscosity within the mixed layer. A comparison of the NBC rings simulated in the CLIPPER experiment with observed ones suggests that the downward penetration of the turbulent kinetic energy is also insufficient. There are not enough subsurface observations available in the Caribbean Sea to have a precise idea of the three dimensional structure of the eddies in this region. However, as it was mentioned in the introduction, observations of Silander (2005) show that some eddies can reach 1000 m. The Caribbean eddies in the CLIPPER model are very shallow, since the deepest ones reach only 300 m.

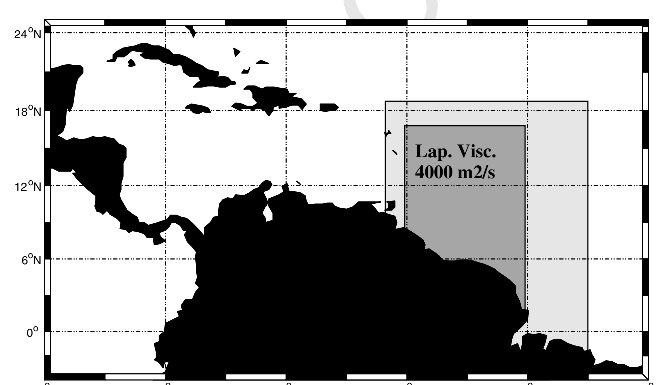

Fig. 3. The dark box represents the region where a strong Laplacian eddy viscosity (4000 $m^2\,s^{-1}$ in NATL3 and 600 $m^2\,s^{-1}$ in CAR15) is added, decaying exponentially to 0 at its edges. The decay is made on the clear gray area. Note that values for bilaplacian viscosity remain unchanged.

2.6. Parent vs. child grid solution

This work is the first 2-way application of AGRIF refinement in NEMO for a configuration which includes free-surface, partial steps and domain breaking-down approach for massively parallel computers. It is therefore of interest to value the efficiency of the system. Snapshots of surface relative vorticity calculated with both coarse (NATL3) and fine grid (CAR15) data from NOSLIP are compared in Fig. 4a and b. We recall that NOSLIP is a 2-way experiment where CAR15 interacts with NATL3, following the procedure described in Section 2.2. Fig. 4a shows only the coarse grid solution, whereas in Fig. 4b the fine grid solution is drawn in the refined domain (the Caribbean region). The meridional black line near 58°W represents the boundary between fine and coarse grids. Due to the difference of resolution, the fine grid solution (Caribbean region in Fig. 4b) produces structures of smaller scale than the coarse grid (Fig. 4a).

Fig. 4a is not an averaging at a 1/3° of Fig. 4b, but is the solution calculated by the 1/3° grid with an update on the CAR15 domain of its SSH and 3D field by the 1/15° solution. It illustrates the effect of updating the parent grid from results of the finer (child) grid shown in Fig. 4b. First note that the two figures are very similar in the refined region, even for location of filaments. Second, the coarse grid solution (Fig. 4a) exhibits a difference of scale in its own domain: the solution over the refined domain is finer than in the Atlantic. Such results can be contrasted with the COARSE

Please cite this article in press as: Jouanno, J. et al., The mesoscale variability in the Caribbean Sea. Part I: Simulations ..., Ocean Modell. (2008), doi:10.1016/j.ocemod.2008.04.002

experiment (1/3°) in Fig. 4c, which was carried out without AGRIF, and produces coarser features.

Although by increasing the model horizontal resolution, the behavior of the Caribbean eddy field becomes more chaotic, a feature in some way illustrated by comparing the snapshots in Fig. 4, the horizontal width of the eddies in the Colombia Basin (where they reach their maximum width), is quite similar for all the experiments (∼500 km). It is not clear whether such scale is bounded and set by the meridional width of the basin or if it corresponds to an intrinsic equilibrium scale of the mesoscale eddies in this region.

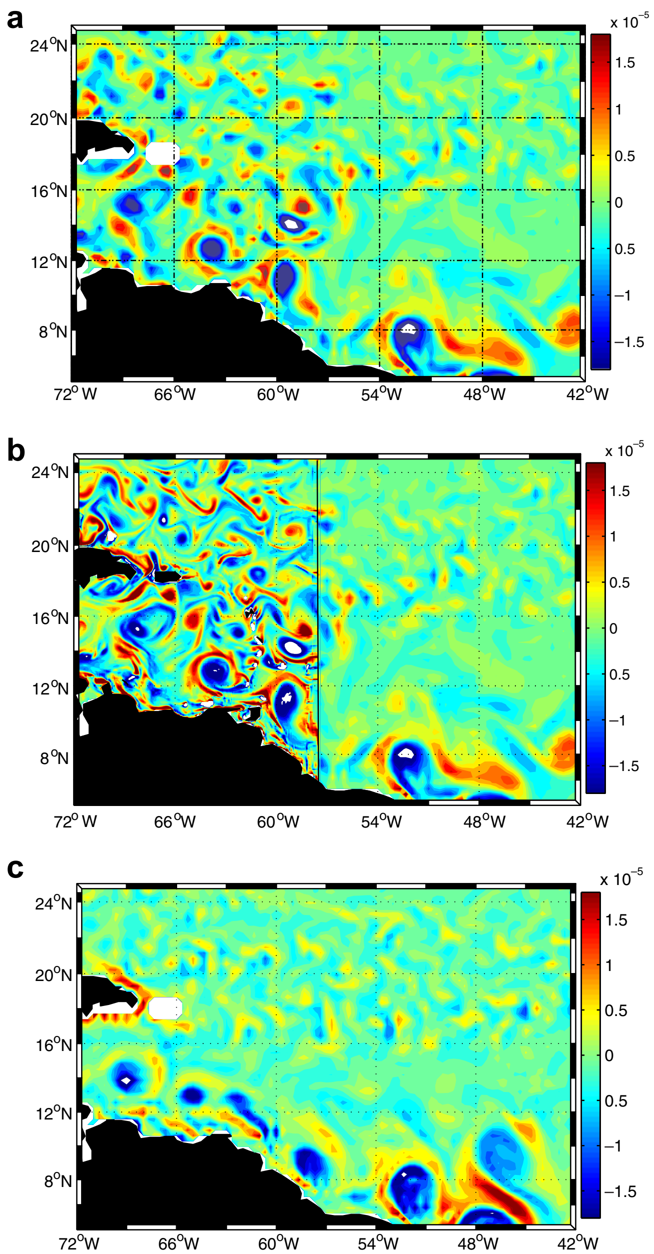

Fig. 4. Snapshots of surface relative vorticity (s^{-1}) for day 6 June of model year 6. (a) Coarse grid solution from NOSLIP experiment; as explained in Section 2.2, the fine grid elliptic solution is interpolated on the corresponding domain in the coarse grid. (b) Child grid solution from NOSLIP experiment superimposed on the parent grid solution plotted in (a). (c) Solution from COARSE experiment (no refined). The vertical black line near 58°W in (a) and (b) shows the eastern boundary of the refined region. Snapshot in (c) does not exactly match the two others since experiments are different.

3. Mean flow

3.1. Current paths

From here on we will focus on the high resolution grid CAR15. Before analyzing the eddy field we describe the upper mean flow produced by the model, starting with the Caribbean inflow. The mean flow is calculated with 6 years of model output from NOSLIP and Fig. 5 shows its structure at 30 and 150 m depth. The mean current paths near the Lesser Antilles at 30 m depth are very different from the current paths at 150 m depth. This illustrates the distinct nature of the two main Atlantic contributions to the Caribbean circulation: the return flow of the MOC and the southern branch of the Subtropical Gyre.

At 30 m depth, the Caribbean inflow is dominated by a narrow and strong flow through the Grenada Passage and a secondary flow through St Vincent and St Lucia Passages. Entering the Venezuela Basin, both branches spread and lie near 65°W–13.5°N. These two surface jets (less than 150 m depth in the model) are similar to those observed with drifter data (Richardson, 2005, his figure 7). They have a clear signature in maps of mean SSH, as seen in Fig. 6 for model mean SSH and observed mean SSH derived from drifters (Niiler et al., 2003). Surface Mean kinetic energy (MKE) map in Fig. 7 illustrates well that this inflow is very energetic. Quasi geostrophic potential vorticity (QGPV) sections discussed in part II of this work will show that in the model: (a) they are part of the upper layers return flow of the MOC, itself formed by waters from the North Equatorial Current (NEC) and the Guyana Current; (b) the instability of the jet flowing out Grenada Passage is mainly responsible for the strong Venezuela (and hence Caribbean) eddy production. At 150 m depth in Fig. 5, Atlantic currents are zonal and meridionally spread, resulting in a more uniform intermediate (from 100 to 500 m depth) contribution to the inflow from St Vincent to Hispaniola. This deeper second main inflow is the southern branch of the Subtropical Gyre, itself part of the Sverdrup transport in the North Atlantic interior. At 150 m depth, note that the strong inflow through the Grenada Passage is absent. The fact that the Caribbean Sea receives these two contributions is well known (e.g., Schmitz and McCartney, 1993), but we will see that their interaction and merging contribute to the growth of strong and deep baroclinic eddies.

Looking now at the flow within the Caribbean proper, one finds strong geographical variations. At 30 m depth in Fig. 5, the main inflow follows the South American coast. Comparing the mean flows at 30 and 150 m depth at 66°W, we can see that the main Caribbean Current (from here on referred to as southern Caribbean Current; sCC) is formed by the merging of the surface flow with the deeper St Vincent to Guadeloupe Passages inflows, as commented previously. The sCC flows westward and reaches Maracaibo, where it has a slight northward deflection. This deflection, due to the geography of the coast line, produces a local velocity maximum. The surface MKE in Fig. 7 illustrates well this local acceleration of the currents. The flow continues west and strikes the Nicaraguan coast. Then it divides into two branches. The southward branch feeds the cyclonic Panama–Colombia Gyre which in turn feeds (a) the sCC main Caribbean Current between 75°W and 78°W, and (b) the Caribbean Coastal Undercurrent (CCU) which is an eastward coastal subsurface flow described by Andrade et al. (2003) and located between 100 and 250 m depth. The northward branch, larger than the southward branch, divides itself into various flows which merge into the Cayman Basin after they have passed through different channels located between Jamaica and Nicaragua. A strong zonal jet is formed and continues westward, strikes the Yucatan coast and becomes the Yucatan Current. Note the permanent anticyclonic circulation south of Cuba, consistent with

Please cite this article in press as: Jouanno, J. et al., The mesoscale variability in the Caribbean Sea. Part I: Simulations ..., Ocean Modell. (2008), doi:10.1016/j.ocemod.2008.04.002

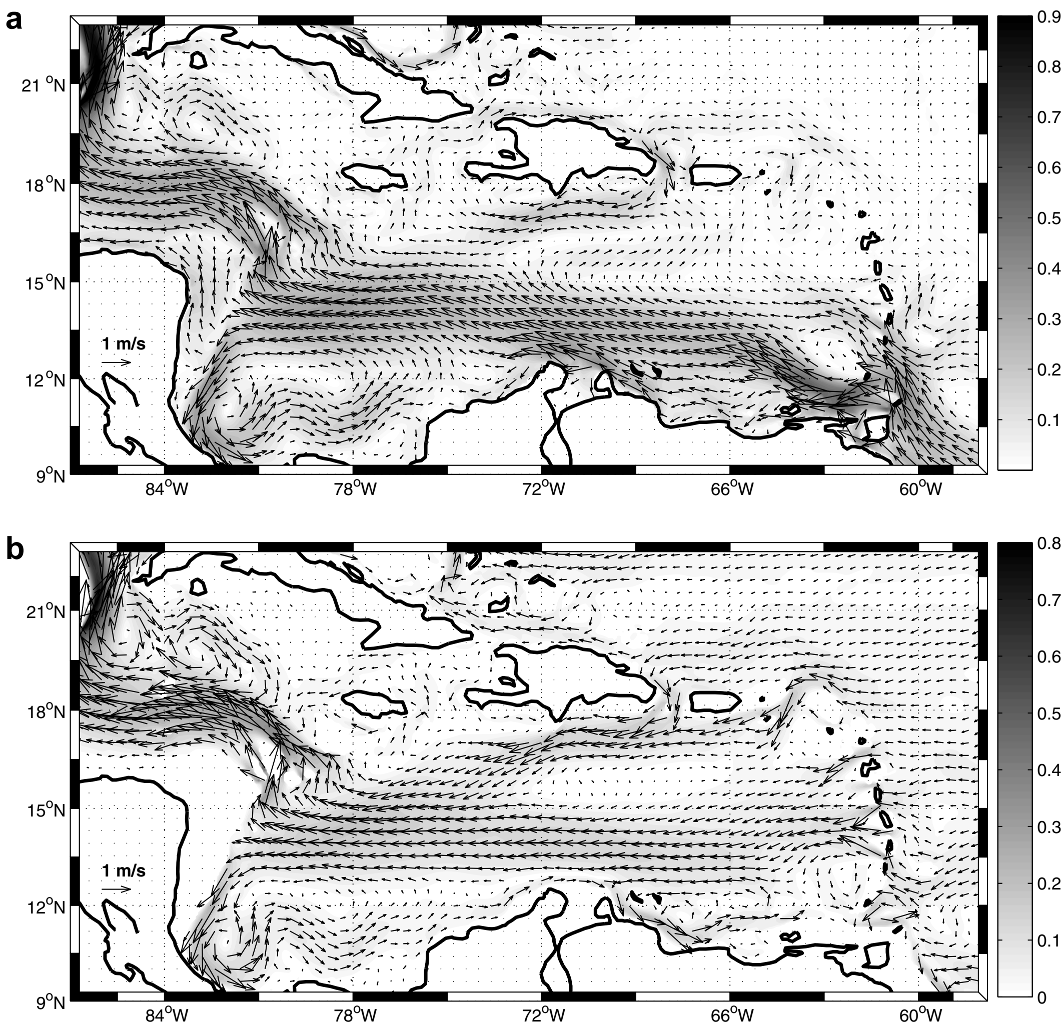

Fig. 5. Mean velocity computed with 6 years of "NOSLIP" model data at (a) 30 m depth and (b) 150 m depth (m s^{-1}). Gray scale indicates magnitude of velocity. The main current is not homogeneous along its path through the Caribbean Sea, indeed some regions present local velocity maximum. The vertical extents of the main core reaches 200 m depth in the Colombia and Venezuela Basin and more than 700 m depth in the Cayman Basin. Comparison between the figures allows to identify the two main contributions to the Caribbean Current: at 30 m depth the strong surface inflow through Grenada Passage is associated with the return flow of the Meridional Overturning Circulation and at 150 m depth the diffuse inflow through the Lesser Antilles Passages is the southern branch of the North Atlantic Subtropical Gyre.

ubiquitous eastward drifter trajectories south of Cuba in Richardson (2005) (see his Fig. 14). The vertical extent of the core of the main Caribbean current is also variable: in the Venezuela and Colombia Basins it reaches 200 m depth, whereas in the Cayman Basin it reaches more than 700 m depth. In its main core, surface speeds are around 0.08 m s^{-1}, though in some regions they can be higher: 0.5 m s^{-1} in Grenada passage or 1 m s^{-1} along the Yucatan coast. All these model features of the main upper Caribbean Current system are in good agreement with drifter observations (Centurioni and Niiler, 2003; Richardson, 2005). A comparison between model and observed mean SSH in Fig. 6 shows that, qualitatively, many features of the Caribbean mean flow are ubiquitous in observation and model. We can give some examples: a separation of the inflow in two surface jets near 62°W, a zonal sCC centered between 3°N and 5°N, a cyclonic Panama–Colombia Gyre which presents two local minima of mean SSH, a maximum of mean SSH in the Cayman Sea. Nevertheless, Fig. 6 also shows that the meridional gradients of model mean SSH are lower than the observed one. It indicates that the mean surface currents in the model are lower than the observed currents.

Model outputs show some secondary currents which are also consistent with observations. In Fig. 5, south of Hispaniola and Puerto Rico, a westward Northern Caribbean Current (nCC) merges at 76°W with the sCC. This jet was observed with drifters (Centurioni and Niiler, 2003; Richardson, 2005). In Richardson (2005) the current appears to originate near the Lesser Antilles at 17°N. In the model, the westward jet seen at 30 m depth south of Hispaniola, appear to be part of an anticyclonic circulation around the eastern side of the island. There are no available observations which could allow us to assess the realism of this anticyclonic pattern and its associated permanent surface cyclone trapped just north of Mona Passage. At 150 m depth, the anticyclonic circulation disappears and without doubt the nCC in the model is fed by waters which enter through Anageda and Mona Passages. Note how the flow (part of the Subtropical Gyre) which gives rise to the nCC is diffuse in the Atlantic and how it organizes in a thin jet south of the Greater Antilles once it enters the Caribbean Sea. It is probable that such structure results mainly from an equilibrium between the nCC and cyclonic eddies which grow on its cyclonic shear.

As remarked by Richardson (2005), this large variety of surface flows in the Caribbean Sea suggests different current regimes. Variability is often related to the mean flow in which it is embedded, so geographical variations and regional differences in the charac-

Please cite this article in press as: Jouanno, J. et al., The mesoscale variability in the Caribbean Sea. Part I: Simulations ..., Ocean Modell. (2008), doi:10.1016/j.ocemod.2008.04.002

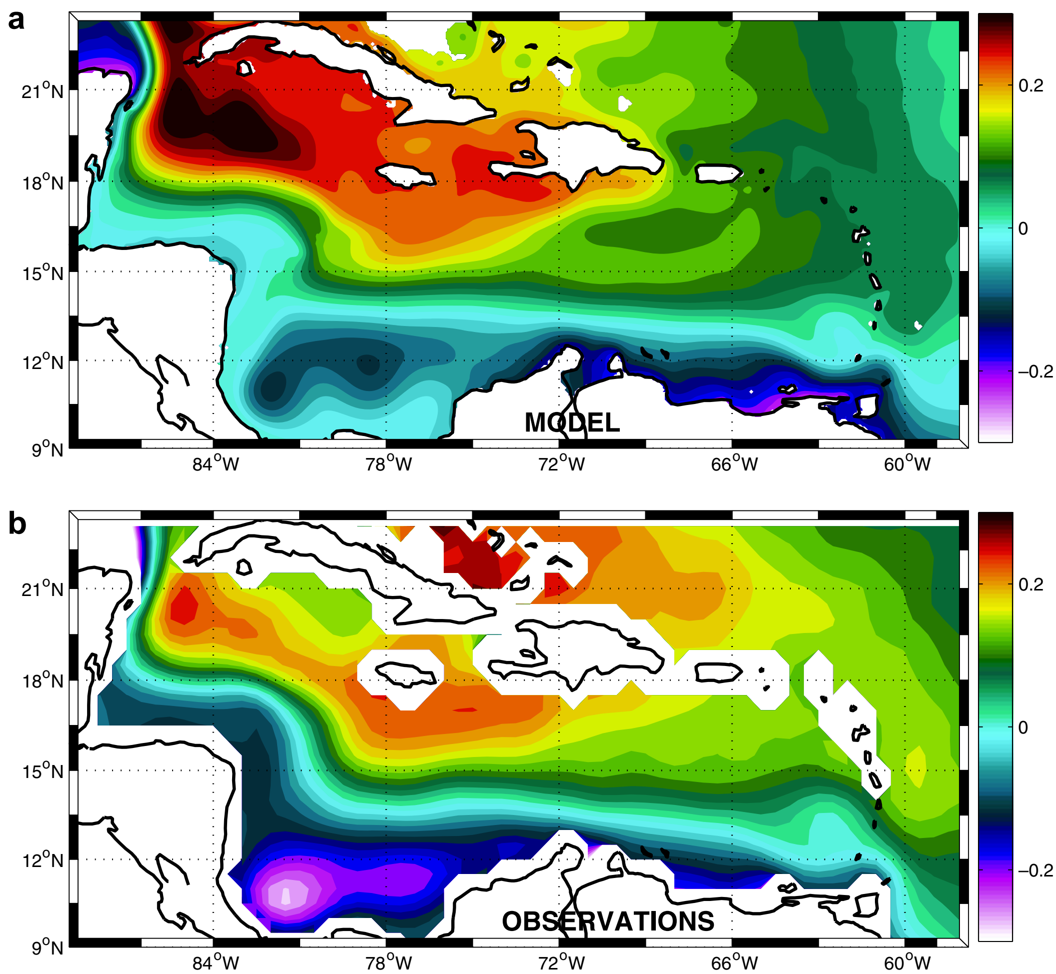

Fig. 6. (a) Mean SSH (m) computed with 6 years of "NOSLIP" model data. (b) The 1992–2002 mean absolute SSH (m) derived from near surface velocity observations as described in Niiler et al. (2003). For both plots, the mean SSH was referenced with respect to a value calculated as the horizontal average of the SSH on the domain plotted in the figures.

teristics of the eddy field can be expected. Such differences will be highlighted in Section 4.1.

3.2. Meridional cross section

Cross sections at 66°W of mean zonal velocity, salinity, potential temperature and potential density are shown in Fig. 8. They correspond to the September/October period. They are compared with observations from Hernández-Guerra and Joyce (2000) (hereafter HJ00) along the same cross section during the same period of the year. We have reproduced the zonal velocity observed by HJ00 in Fig. 8e and the potential density in Fig. 8f. The structure of the mean zonal flow (Fig. 8b) is consistent with most of the patterns shown by the in situ observations:

- An intense and shallow westward flow is centered at 66°W in both model and HJ00 sections. In HJ00, the zonal velocity reach speeds up to 1 m s^{-1} whereas for the model, surface velocity does not reach 0.3 m s^{-1}. The observations were carried out during the shedding of a large anticyclone (as seen in their Fig. 4), so such energetic event could explain the discrepancy between these maximum velocities. In the upper layers near the continental coast (11°N), the flow is oriented westward in the model whereas it is oriented eastward in observations. We have observed in the model that when a large anticyclone is growing in the Venezuela Basin by instability of the sCC, its cyclonic counterpart grows between the sCC and the continent and that produces an eastward coastal current as observed in HJ00.
- A deep westward current is located at 17.5°N: the nCC (northern Caribbean Current). In both model and HJ00 data, its main core is located roughly down 100 m depth.
- The Caribbean Coastal Undercurrent (see also Andrade et al., 2003) flows eastward between 11°N and 12°N in both observations and model.
- In the center of the section, between 15°N and 16°N, HJ00 observed a slight eastward flow. The model does not represent such pattern. Nevertheless, note that in this same region the strength of the westward flow is minimum.

In both model and observations, a maximum of salinity is centered at 150 m depth. Because of its location north of 13.5°N, this water is probably mostly advected by the subtropical gyre flow. Model potential temperature and potential density (Fig. 8a and d) show patterns consistent with HJ00, in particular an outcropping of the isotherms and isopycnals near the American continent. From surface to 150 m depth, temperatures (density) appear to be lower (higher) in the model in comparison to observations, and the discrepancy does not hold in the standard deviation range (of order 1° in the upper layer for the August–September period). Indeed, the model mixed layer temperature is of 26 °C whereas it reaches 28 °C

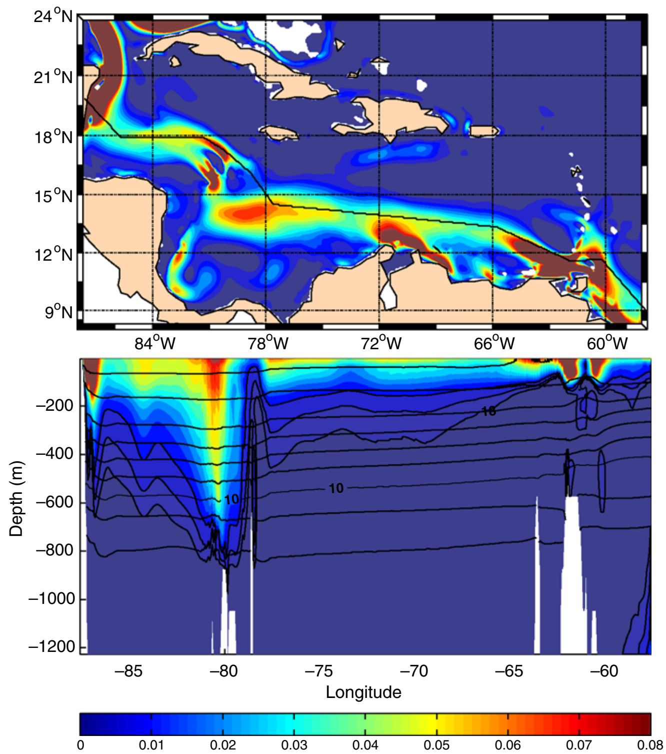

Fig. 7. (a) Model mean kinetic energy (MKE; $m^2 s^{-2}$) calculated as a 6 years average of surface data from NOSLIP. (b) Zonal section of MKE following the black line indicated in (a). Horizontal isolines represent temperature from 8 to 22 °C.

in observations. Such discrepancy is probably due to a lack of realism of the atmospheric forcing.

3.3. Sensitivity to model configuration

In Fig. 9, the mean surface velocity field is given for three other experiments, COARSE (1/3°), CLIPPER (1/6°) and REF (1/15°), and should be compared with mean surface velocity field from NOSLIP (1/15°) shown in Fig. 5a and mean surface velocity inferred by drifters in Richardson (2005) (his Fig. 7). Various patterns are better represented in NOSLIP:

- The separation of the surface inflow between Grenada and St Vincent–St Lucia Passages is only seen in NOSLIP. In CLIPPER and COARSE, this inflow is broader and its acceleration through Grenada Passage is not clear. Such difference has certainly an impact on the eddy formation in this region, since it will be seen in part II that most of the large eddies are triggered in this region. In REF there is a kind of separation but the flow which enters through St Vincent continues more north and does not connect with the Grenada inflow as seen for NOSLIP in Fig. 5.
- Outside the Caribbean Sea, a weak surface mean flow along the Lesser and Greater Antilles from Grenada to Hispaniola can be seen in NOSLIP but not in REF. In the following section, comparison of surface mean eddy kinetic energy (MEKE) maps will indicate that the eddy activity in this region is much more intense in NOSLIP than in REF. It suggests that mean flow and eddies are closely linked in this region.
- The nCC is obvious only in NOSLIP and REF. In COARSE, a thin westward circulation occurs just south of Hispaniola, but appears to be part of an anticyclonic circulation which occurs around the island. So it might not be produced by waters coming directly from the Subtropical Gyre, as it appears to be in NOSLIP. A striking feature is that such anticyclonic circulation in COARSE occurs as well around Jamaica and Cuba in a lesser extent. We think these patterns are artifacts of the model, caused by a non adequate resolution of the barotropic streamfunction near the islands. In CLIPPER there is no nCC at 30 m depth, but at 130 m depth a westward flow exists (not shown) and could be associated with the nCC. Such differences indicate the strong sensitivity of the north Caribbean circulation to resolution and model configuration. Following, such sensitivity is confirmed by comparing barotropic transports.
- The acceleration of the mean flow just north of Maracaibo (70°W–14°N) is ubiquitous in the four experiments. We link this with the MEKE increase which occur in all the experiments in this region. Topographic effects favor the acceleration of the sCC and hence the growth of the eddies formed generally more to the east and embedded in this current.
- The shape of the cyclonic Panama–Colombia Gyre is also model dependent. In COARSE the circulation in this region is formed by an unique broad cyclonic flow accelerated near the coast whereas in CLIPPER two cells can be distinguished: one which closes the gyre near 80°W and another which joins the sCC near 76°W. In NOSLIP and REF, there are also two cells but note how the southern flow of the largest cell is meandering. These meanders are due to a quasi permanent presence of a triad of eddies: a cyclone, an anticyclone and a cyclone. Such triads have been observed by Andrade and Barton (2000).
- Between Jamaica and Nicaragua, the separation of the flow into two jets only occurs in NOSLIP and REF. There are no observations available to validate such behavior.
- The permanent anticyclonic gyre south of Cuba, which has been inferred with drifter data in Richardson (2005), is only simulated in NOSLIP and REF.

We have shown how by increasing resolution, the mean current paths are improved. An increase of the horizontal resolution affects the mean flow in three main ways: first, it affects the mean currents by modifying their interaction with the coast and their horizontal diffusion (it allows finer structures). Second, a better resolution of topography and Antilles Passages modifies the paths of the inflow. We will show in Section 4.1 that the behavior of Atlantic eddies and waves that reach the Caribbean Sea is also resolution dependent. Third, since the eddy field is resolution dependent and is expected to interact with the mean field, different resolutions of the eddy field might also influence the current paths. It is probable that eddies provide a flux of momentum which favor the organization of the Caribbean currents in jets. We should not forget that the Caribbean circulation is an equilibrium between an eddy field and a mean flow, so a better resolution of the mean field and mean inflow might also influence the characteristics of the eddy field (e.g., through the behavior of the NBC rings, the vertical and horizontal shear in the Grenada Passage or the strength of the nCC).

3.4. Barotropic transport

Transport is computed for different sections to get more insight on how AGRIF, horizontal resolution and boundary conditions influence the inflow and current paths in and out the Caribbean Sea. Transport sections are indicated in Fig. 10. Barotropic transport is compared to observational data (when available) in Table 3.

One important result is that grid refinement modifies the paths of the large scale circulation in the region. In COARSE, the transport through Yucatan reach 28 Sv whereas in AGRIF configurations this transport is lower (e.g., 20.3 Sv in NOSLIP and 23.4 Sv in REF). The transport through the section between Puerto-Rico and Venezuela shows smaller differences between experiments (COARSE −18.5 Sv, NOSLIP −19.1 Sv and REF −22.1 Sv) and agrees with

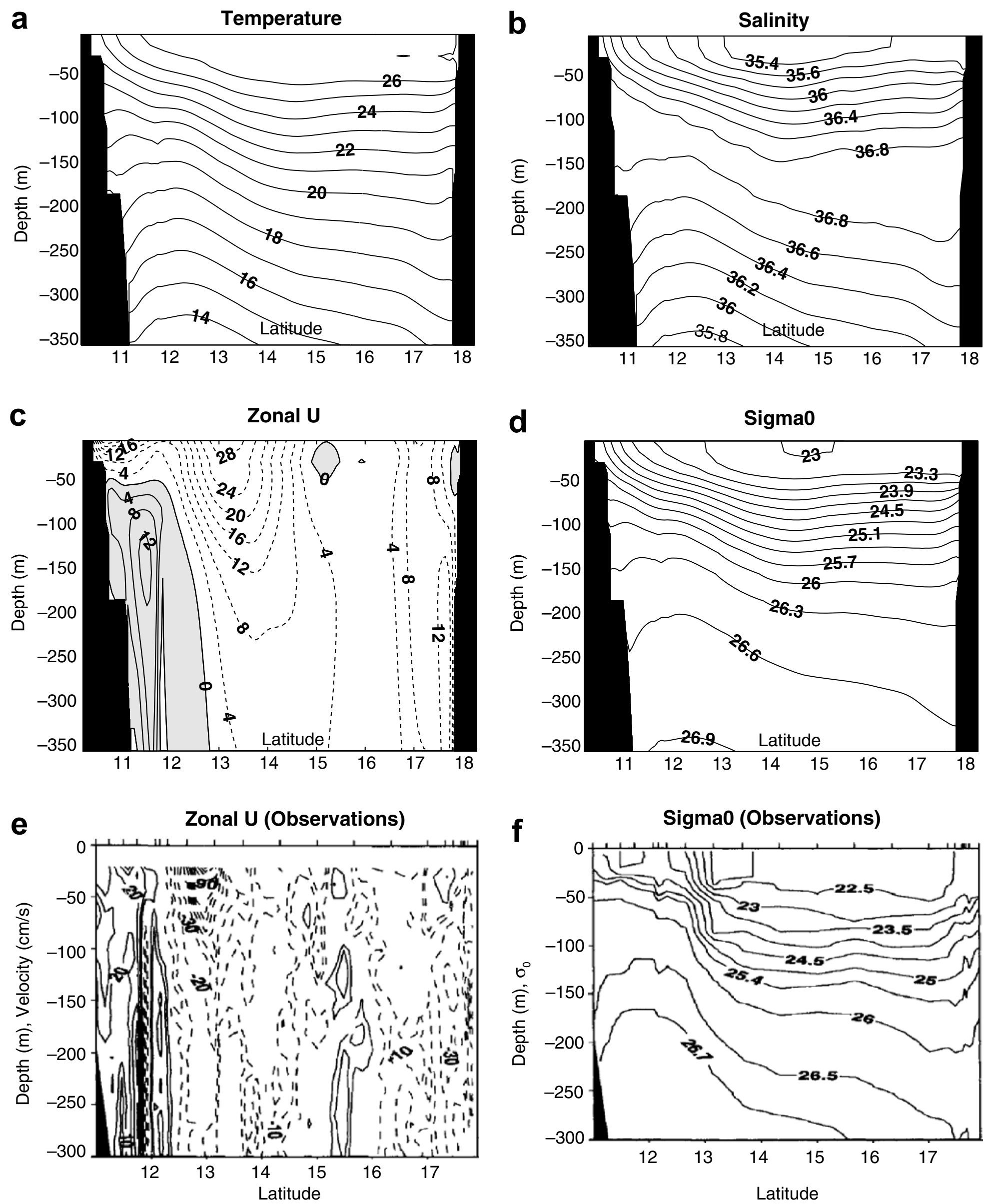

Fig. 8. Meridional cross section at 66°W during August/September of (a) potential temperature (°C), (b) salinity, (c) mean velocity (m s^{-1}, gray colored values represent an eastward transport) and (d) potential density. Plots are based on an average for the period September/October calculated with 6 years of data from NOSLIP experiment. These sections are compared with in situ observations from Hernández-Guerra and Joyce (2000) at 66°W: (e) zonal velocity (cm s^{-1}) from VMADCP and (f) potential density.

the 18.4 ± 4.7 Sv estimated with observations in Johns et al. (2002). Note that through this section the transport in COARSE is lower than in NOSLIP, whereas through the Yucatan section the contrary occurs. So, the difference of transport through Yucatan Channel is mainly due to strong difference between transports through the Greater Antilles Passages (Mona and Windward Passages). Indeed the mean flow through Windward Passage is an inflow in some experiments (e.g., MEAN, COARSE, CLIPPER) and an outflow in others (e.g., REF and NOSLIP). Transports through Windward Passage, inferred with a current meter array deployed across the passage during 17 months (Smith et al., 2007), range approximately from −5 to 15 Sv, with an average inflow of 3.6 Sv. Neither the strength of the mean flow through the passage, nor its strong observed variability are correctly represented by the different numerical experiments. In addition results appear to be highly model dependent. Because of its northern location we expect that the inadequate simulation of the flow through this passage does not affect too much the behavior of the Colombia/Venezuela eddies. Nevertheless, such discrepancy with observations are considered as serious and the solution of the model in this region has to be improved.

The zonally integrated streamfunction indicates that the strength of the MOC is low in the model: its amplitude through the Equator and the North Atlantic is about 10 Sv whereas observations of Talley et al. (2003) show an overturn with an amplitude of about 18 Sv (error of order 3–5 Sv) through most of the Atlantic. In addition to the misrepresentation of the inflow through Windward Passage, it could explain that the transport through Yucatan (20.3 Sv in NOSLIP) is lower than the observed one (23.8 Sv, Sheinbaum et al., 2002).

The transport between Florida and the Bahamas Bank has been estimated with a submarine cable at 27°N by Larsen (1992), they found a mean transport equal to 32.3 Sv, and at 26°N by Niiler and Richardson (1973) who found a mean transport of 29.3 Sv. There is a strong discrepancy between these values and the

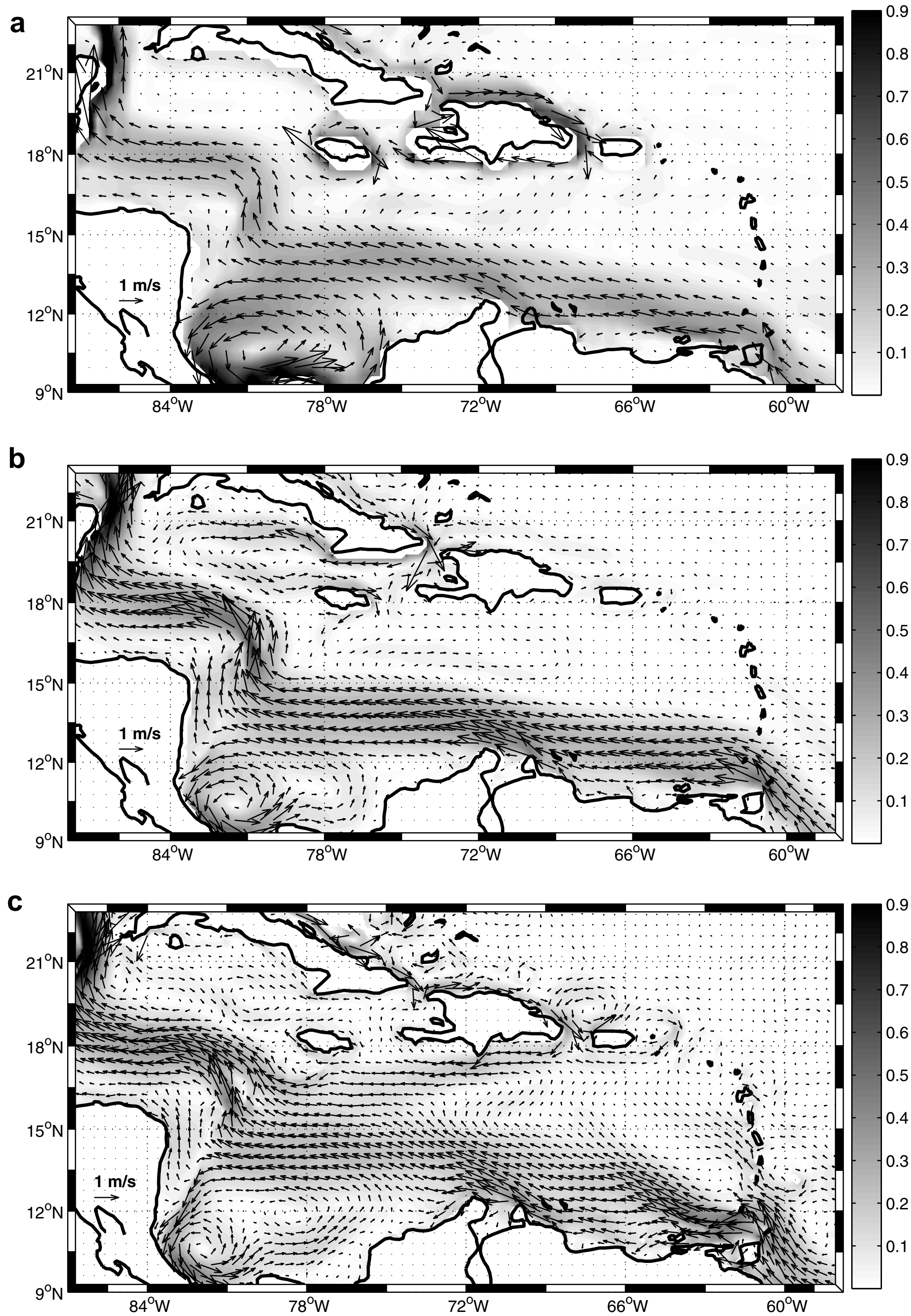

Fig. 9. Mean velocity field (m s^{-1}) at 30 m depth, computed with 6 years from the experiments COARSE (a), CLIPPER (b) and REF (c). Note that for better clarity, we have not plotted all the vectors.

observed 23.8 Sv through the Yucatan Channel (Sheinbaum et al., 2002). A natural question arises regarding the origin of the 6 Sv which should feed the current somewhere between Yucatan Channel and Florida Straits. The two main Passages are the Old-Bahamas Passage and North-West providence passage. Observed transport through these sections appear to be small: L-ADCP sections of (Johns, 2007) indicates that transport in the Old-Bahamas Passages is low and that the direction of the flow is inverted in the vertical (eastward at 20 m depth and westward at 200 m depth); Leeman et al. (1995) inferred a transport of −1.2 Sv through the North-West Providence Passage. So, it remains an open question. Unfortunately, the model does not bring any answer to this problem, since the transport at 27°N (e.g., 23.6 Sv in REF), referred as “Florida Straits” in Table 3, is almost equal to the transport through Yucatan Channel (e.g., 23.4 Sv in NOSLIP).

The circulation outside the Caribbean is also affected by model configurations since at 17.7°N there are strong discrepancies: −18.9 Sv in REF, −14.9 Sv in NOSLIP and −21.0 Sv in COARSE. This

Please cite this article in press as: Jouanno, J. et al., The mesoscale variability in the Caribbean Sea. Part I: Simulations ..., Ocean Modell. (2008), doi:10.1016/j.ocemod.2008.04.002

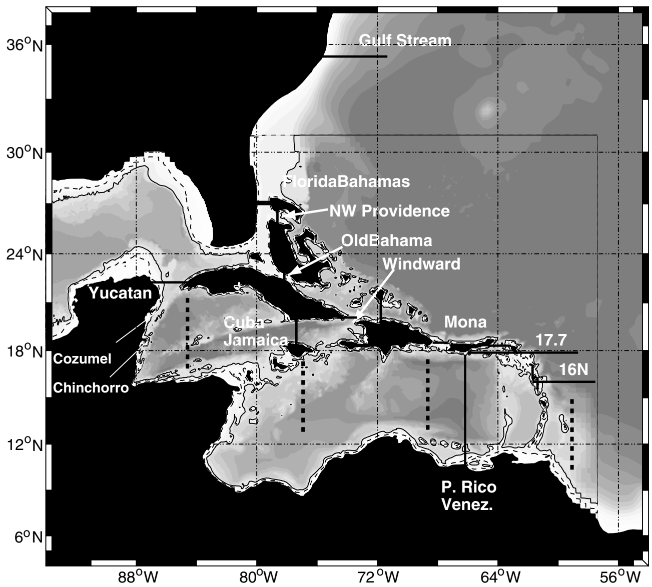

Fig. 10. Sections used to calculate the transports resumed in Table 3. See Fig. 1 to see the location of the Antilles Passages. Dashed black vertical lines represent the sections over which variance conserving spectrum in Fig. 16 are calculated.

transport is dominated by a deep southward western boundary undercurrent which appears to be sensitive to horizontal boundary conditions since NOSLIP shows the lowest transport.

The Gulf Stream section indicates a slight feed back of the fine grid on the coarse grid. The northward transport through this section, equal to 26.9 Sv in COARSE, increases to 27.7 Sv in REF and 29.2 Sv in NOSLIP. The effects of the grid refinement on the MOC have been quantified, but are not significant (not shown).

3.5. Caribbean Coastal Undercurrent

Hydrographic and L-ADCP observations from Andrade et al. (2003) have shown evidences of the existence of a Caribbean Coastal Undercurrent (CCU), which flows eastward along the Central and South American Caribbean coast. The model also represents such current, as shown by the mean flow from NOSLIP at 130 m depth in Fig. 5. The undercurrent is mainly located between 100 and 400 m depth but can have locally deeper contributions as in the Cariaco Basin.

The CCU is part of the wind driven Tropical North Atlantic cyclonic cell. Johns et al. (2002) show that a purely wind forced model produces a cyclonic tropical cell which implies a net transport of 5 Sv to flow eastward along the South American coast. They found that once the MOC is added, no such mean flow exits the Caribbean, and the Panama–Colombia Gyre is the unique pattern which persists. Such calculations are vertically integrated, so they do not contradict the existence of a subsurface Counter Current, but they suggest that the MOC could weaken the eastward transport. Dynamically, the main effect of this undercurrent is to increases the vertical shear of the sCC, and hence the eddy variability by baroclinic instability.

In the calculation, only the eastward velocities are integrated, so the transport estimate does NOT include westward flow. The reason why we limit the integration (of eastward velocities) to 13 N, is because we are interested here in catching the coastal flow only.

The eastward transport has been computed for NOSLIP and REF experiments and shown in Fig. 11. In the calculation, only the eastward velocities are integrated, so the transport estimate does not include westward flow. We limit the integration at 13°N to catch the coastal flow only. Regions with enhanced transport as the Panama–Colombia Gyre (80°W) or the Cariaco Basin (67°W) are regions of recirculation (as seen in Fig. 5 at 130 m depth). The outflow through the Grenada passage, near 62°W is about 1 Sv for both experiments and is located mainly between 100 and 400 m depth. It agrees with the 1 Sv outflow estimated in Andrade et al. (2003). In the Guajira region (72°W, see map in Fig. 1), the eastward flow in NOSLIP is about 1 Sv. The strength of the eastward coastal flow, in particular in regions of recirculation is strongly dependent on the horizontal boundary condition. The use of no-slip boundary conditions (NOSLIP) reduces by half the eastward transport in these regions in contrast to the transport obtained with free-slip boundary conditions (REF). Note that the outflow through Grenada Passage is less affected, since it transports nearly 1 Sv in both REF and NOSLIP experiments. The comparison of mod-

Table 3
Barotropic transport (Sv, 1 Sverdrup = 10^6 m^3 s^{-1}) for sections described in Fig. 10 calculated for each experiment with 6 years of model data

Experiment	REF	NOSLIP	MEAN	VISC	COARSE	Clipper	Obs	Sources
Yucatan	23.4 ± 1.2	20.3 ± 1.2	21.6 ± 0.9	23.8 ± 1.3	28.2 ± 1.4	26.1 ± 3.5	23.8	Sheinbaum et al. (2002)
Florida–Bahamas	23.8 ± 1.6	21.2 ± 1.2	23.0 ± 1.4	23.7 ± 1.4			32.3 (at 27°N)	Larsen (1992)
NW-Providence	−0.8 ± 1.2	−1.1 ± 0.7	−0.9 ± 1.2	−0.2 ± 1.3			−1.2	Leeman et al. (1995)
Old-Bahama	0.7 ± 0.6	0.5 ± 0.5	−0.2 ± 0.6	0.6 ± 0.7				
Windward	0.6 ± 2.2	1.1 ± 2.2	−0.4 ± 1.9	1.7 ± 2.1	−2.4 ± 1.9	−7.5 ± 3.9	−3.6 (from −15 to 5)	Smith et al. (2007)
Cuba–Jamaica	0.9 ± 3.6	−1.3 ± 2.6	0.6 ± 3.2	2.0 ± 2.9		4.6 ± 5.0		
Mona	−2.1 ± 1.1	−2.6 ± 0.9	−2.6 ± 0.8	−2.3 ± 1	−2.6 ± 1.2	−1.4 ± 1.5	−2.6	Johns et al. (2002)
Anageda	−4.4 ± 1.9	−4.4 ± 2.0	−3.8 ± 1.9	−5.4 ± 1.6			−2.5 ± 1.4	Johns et al. (2002)
Hispaniola	0.9 ± 5.0	−0.4 ± 3.1	0.7 ± 1.9	−1.2 ± 3.7				
Antigua	−2.0 ± 1.2	−2.0 ± 0.9	−2.4 ± 1.0	−1.7 ± 0.4			−3.1 ± 1.5	Johns et al. (2002)
Guadeloupe	−0.7 ± 1.0	−1.3 ± 0.5	−1.0 ± 0.9	−0.9 ± 0.3			−1.1 ± 1.1	Johns et al. (2002)
Dominica	−5.1 ± 1.5	−3.4 ± 1.0	−5.0 ± 1.4	−5.4 ± 0.9			−1.4 ± 1.1	Johns et al. (2002)
St Lucia	−1.6 ± 0.8	−1.0 ± 0.6	−1.5 ± 0.6	−1.5 ± 0.4			−1.4 ± 2.0	Johns et al. (2002)
St Vincent	−2.5 ± 1.0	−2.0 ± 0.7	−1.7 ± 0.9	−2.8 ± 0.6			−3.2 ± 2.1	Johns et al. (2002)
Grenada	−4.3 ± 2.1	−3.6 ± 1.6	−2.0 ± 1.5	−4.3 ± 1.6			−5.0 ± 2.8	Johns et al. (2002)
GulfStream	27.7 ± 6.2	29.2 ± 7.8			26.9 ± 9.7			
16 N	−19.0 ± 8.2	−17.3 ± 9.7	−14.8 ± 7.0	−18.3 ± 3.4				
17.7 N	−18.9 ± 7.4	−14.9 ± 13.3			−21.0 ± 6.4			
P-Rico-Venez	−22.2 ± 2.2	−19.0 ± 2.3	−18.8 ± 1.9	−23.5 ± 2.5	−18.5 ± 0.8	−18.9 ± 3.5	−18.4 ± 4.7	Johns et al. (2002)
Cozumel	3.0 ± 0.5	1.6 ± 0.3	2.8 ± 0.3	3 ± 0.4				
Chinchorro	3.5 ± 1.2	2.1 ± 0.8	3.5 ± 1.0	3.4 ± 1.4				

Positive values for zonal (meridional) sections represent a northward (eastward) transport.

Please cite this article in press as: Jouanno, J. et al., The mesoscale variability in the Caribbean Sea. Part I: Simulations ..., Ocean Modell. (2008), doi:10.1016/j.ocemod.2008.04.002

el data with observations from Andrade et al. (2003) suggests that the CCU is better resolved in REF, but note that there a no long term observations available to give us confidence on the real the structure of the CCU.

4. The eddy field

4.1. Instantaneous eddy field

A snapshot of surface horizontal velocities from NOSLIP, shown in Fig. 12, highlights some characteristic features of the eddy field in the model. A baroclinic NBC ring surrounds Barbados at 60°W in the Atlantic Ocean (shown as A on the figures). The vertical section shows that its energetic core reaches down to 200 m depth and a slight velocity anomaly extends down to 1100 m depth. CTD and L-ADCP sections at 16°N allowed to observe two anticyclones with the same characteristics (Rhein et al., 2005). In the same study, they also report an anticyclone which is subsurface intensified with its main core centered at 400 m depth. The model produces such subsurface features (not shown). All these similarities and particularly the deep vertical extent of the NBC eddies give some confidence about the representation of the physics by the model outside the Caribbean, and in due course inside the Caribbean. The CLIPPER experiment (e.g., Candela et al., 2003), which was commented before, used an older version of the code, produced shallower eddies at these latitudes. It seems that the improvement seen here results from both implementation of a new momentum advection scheme and a better representation of the bottom topography with the utilization of partial bottom cells (Barnier et al., 2006; Penduff et al., 2007).

West of the Lesser Antilles at 65°W, an eddy pair (B) is growing and being advected northward. It was not produced by an NBC ring (not shown), but was born just west of the Grenada Passage, in the core of the strong inflow (C). The vertical extent of the eddy pair is still shallow (300 m depth), as shown in the vertical section. Further west, two larger (diameter between 300 and 400 km) anticyclonic eddies (D) of deeper vertical extent are traveling westward. Although their main cores are limited to 200 m depth, both reach 1000 m depth. From the Lesser Antilles to 72°W, cyclonic eddies develop and travel near the South American coast, they usually constitute the cyclonic counterpart of the large Caribbean anticyclones and are weaker than the anticyclones. In Fig. 12, a westward jet (E) is observed south of Hispaniola, in agreement with the mean flow in this region (see Fig. 5). Although it is not illustrated on the figure, cyclonic eddies are sometimes formed on its cyclonic flank and are rapidly dissipated or destroyed under the influence of the large and persistent southern Caribbean anticyclones. Reaching the channels between Jamaica and Nicaragua, the flow accelerates (F) and becomes more barotropic. Velocities up to 25 cm s^{-1} are found down to 1000 m depth. In these regions, several eddies are embedded in the mean jet. South of Cuba, an anticyclonic eddy is forming (G) and will travel west to the Yucatan coast where it will merge with the Yucatan Current.

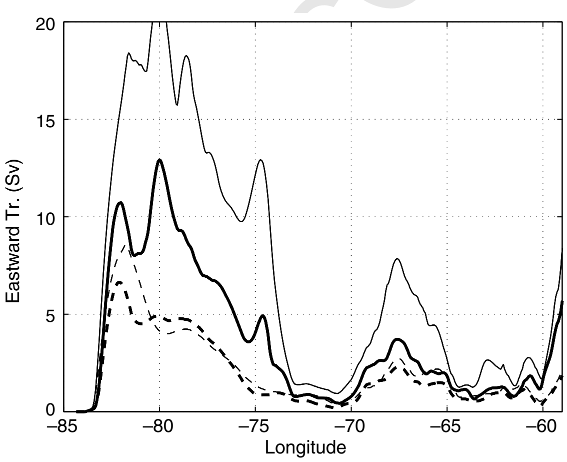

Fig. 11. Eastward mean transport (Sv) from the coast to 13°N for experiment NOSLIP (bold lines) and REF (thick lines). Eastward transport is integrated from the surface to 415 m (dashed lines) and from the surface to the bottom (full lines).

4.2. MEKE field

Surface mean eddy kinetic energy (MEKE) calculated with 6 years of NOSLIP experiment data is compared with the MEKE calculated with 5 years of surface geostrophic velocity anomalies derived from AVISO altimeter data. The MEKE is computed from surface velocity anomalies (u', v') with respect to a temporal mean of the surface velocity field. In Fig. 13, the surface model MEKE (Fig. 13a), calculated directly with velocities from the fine grid (1/15°), is of same order as the MEKE calculated by Richardson (2005) with drifters observations (212 drifters from 1998 to 2000). He found that high values of MEKE (>0.08 m^2 s^{-2}) are prevalent in the central Venezuela and Colombia Basins and in a few areas of the Yucatan and Cayman Basins, coherent with the values of our model, as seen in Fig. 13a. In comparison, altimetry MEKE (Fig. 13c) is less energetic, since it shows values of order 0.05 m^2 s^{-2} in the Colombia and Venezuela Basins. Note that if the MEKE calculation is carried out with geostrophic velocities derived from coarse grid SSH, as shown in Fig. 13d, MEKE values are lower than those obtained from the instantaneous velocity field (Fig. 13a) and closer to those obtained from altimetry. But in general, whatever the way it is calculated, surface MEKE in the model shares many characteristics with the geostrophic MEKE calculated from altimetry data. In particular, MEKE values are of same order and show a westward increase from the Lesser Antilles to the Colombia Basin, region of greater variance. The Panama–Colombia Gyre presents a local maximum of variability near the South American Coast for both altimetry and model data, indicative that local processes enhance the variability in this region. Passing the Chibcha Channel toward the Cayman Sea, the variability of the flow decreases drastically. It was proposed by Andrade and Barton (2000) and Carton and Chao (1999) that the Eastern Caribbean eddies are dissipated by topographic features in the coastal waters of Nicaragua. In addition to such dissipation process, we suggest that in these regions the eddy field loses energy by transferring energy to the mean flow. This is based on the simple observation that regions where the MEKE decreases are regions where the MKE is very strong. Horizontal and vertical sections of MKE plotted in Fig. 7 illustrate well that the Chibcha Channel and especially the Yucatan Channel present a strong MKE. This proposition is supported in part II by calculations of energy conversion terms between mean and eddy field. In the Cayman Sea, MEKE increases northwestward toward a local maximum in the center of the basin, suggesting a local source of energy for the eddy field. Reaching the Yucatan coast and Yucatan Channel, the MEKE decreases again.

The MEKE section along the Caribbean Sea, displayed in Fig. 13c, reveals that the model mainly produces baroclinic structures. The section was made along the trajectory indicated by the black line on the horizontal panel of the same figure. Near the Lesser Antilles, similar values of MEKE are shallower in the Caribbean Sea than in the Atlantic Ocean. The passages of the Lesser Antilles modify strongly the perturbations advected by the NBC. In the interior of the Caribbean, the eddies rapidly deepen westward. Consistent Fig. 13a, the MEKE increases strongly westward toward the Colombia Basin. Note how higher values of MEKE are located in the first 100 m depth, showing the baroclinic character of the Caribbean

Please cite this article in press as: Jouanno, J. et al., The mesoscale variability in the Caribbean Sea. Part I: Simulations ..., Ocean Modell. (2008), doi:10.1016/j.ocemod.2008.04.002

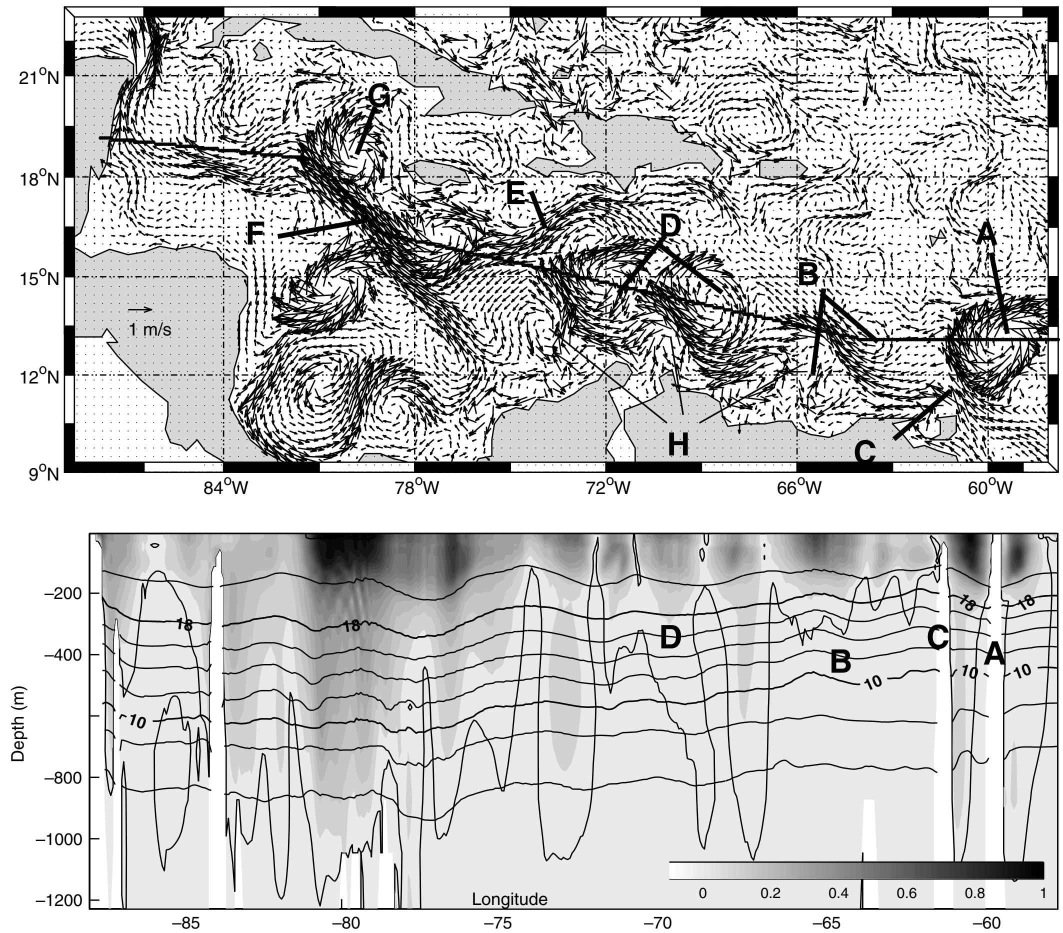

Fig. 12. Instantaneous eddy field: (top) snapshot of the velocity at 30 m depth (m s^{-1}). (bottom) Instantaneous kinetic energy (gray scale, $m^2\ s^{-2}$) plotted along the zonal section indicated with a black line in (top). The thin black line is an isocontour of 0.05 $m^2\ s^{-2}$ kinetic energy. Wide black lines are isotherms (°C). As detailed in the text, such snapshot is characteristic of the upper-layer dynamics of the Caribbean Sea.

eddies. An abrupt deepening of the high MEKE tongue occurs at 77°W, near the Nicaraguan Coast and the Chibcha Channel. In REF simulation, whose unique difference with NOSLIP is to use free slip horizontal boundary conditions, it can be seen that MEKE decreases and the perturbations become shallower when they approach the Chibcha Channel (Fig. 14c). So, we suggest this abrupt deepening is related to a geographic effect of the Nicaraguan coast. The variability presents a minimum in the Chibcha Channel but increases rapidly further west. Although less energetic, the variability in the Cayman Basin deepens rapidly west of the Channel. The mean current, deeper in this region, allows the variability to reach higher depths more rapidly than in the Venezuela Basin. Indeed, it will be shown in part II that the Cayman Current presents a strong horizontal shear at depth down to 500 m depth, which allows deep barotropic instability (i.e. instability produced by horizontal velocity shear).

4.3. Intercomparison of MEKE field in different experiments

Surface MEKE for the four other experiments are shown in Fig. 14. All the experiments share some characteristics, in particular a region of larger variance in the Colombia Basin, consistent with a local maximum of observed SSH rms (e.g., Oey et al. (2003) or Fig. 13), and an east to west increase of the MEKE along the Venezuela Basin, starting from the Lesser Antilles to 70°W. Passing the Chibcha Channel toward the Cayman Sea, the variability of the flow decreases but increases toward a local maximum in the center of the basin. Reaching the Yucatan coast and Yucatan Channel the MEKE decreases again. Now, a careful look at these figures, completed by a comparison with altimetry MEKE and NOSLIP MEKE both shown in Fig. 13, highlights (1) some important differences, which indicate again that NOSLIP is the more realistic simulation, and (2) many robust features, which are safe to interpret since they survive changes of configuration:

- In all the experiments, MEKE just west of the Lesser Antilles is very low, except for CLIPPER in which the band of high MEKE in the Atlantic, due to the northwestward advection of NBC rings, is not broken by the Lesser Antilles. NBC rings in CLIPPER appear to "feel" less the L. Antilles than in the other experiments. It is striking that COARSE, which has a coarser resolution of the L. Antilles Passages than CLIPPER, do show such decrease of the MEKE. This improvement could be the result of: (1) the bottom topography is not represented with partial steps in CLIPPER, so the interaction with the bottom near the Antilles Passages could be better resolved in COARSE despite its lower resolution. (2) In CLIPPER, the NBC rings are shallower than in COARSE, so their behavior when reaching the Lesser Antilles is expected to be different. In particular their crossing through the Passages appears to be easier. These improvements are consistent with results of Penduff et al. (2007) who show that in a 1/4° global model, MKE and MEKE are substantially increased at depth by the use of partial steps.

Please cite this article in press as: Jouanno, J. et al., The mesoscale variability in the Caribbean Sea. Part I: Simulations ..., Ocean Modell. (2008), doi:10.1016/j.ocemod.2008.04.002

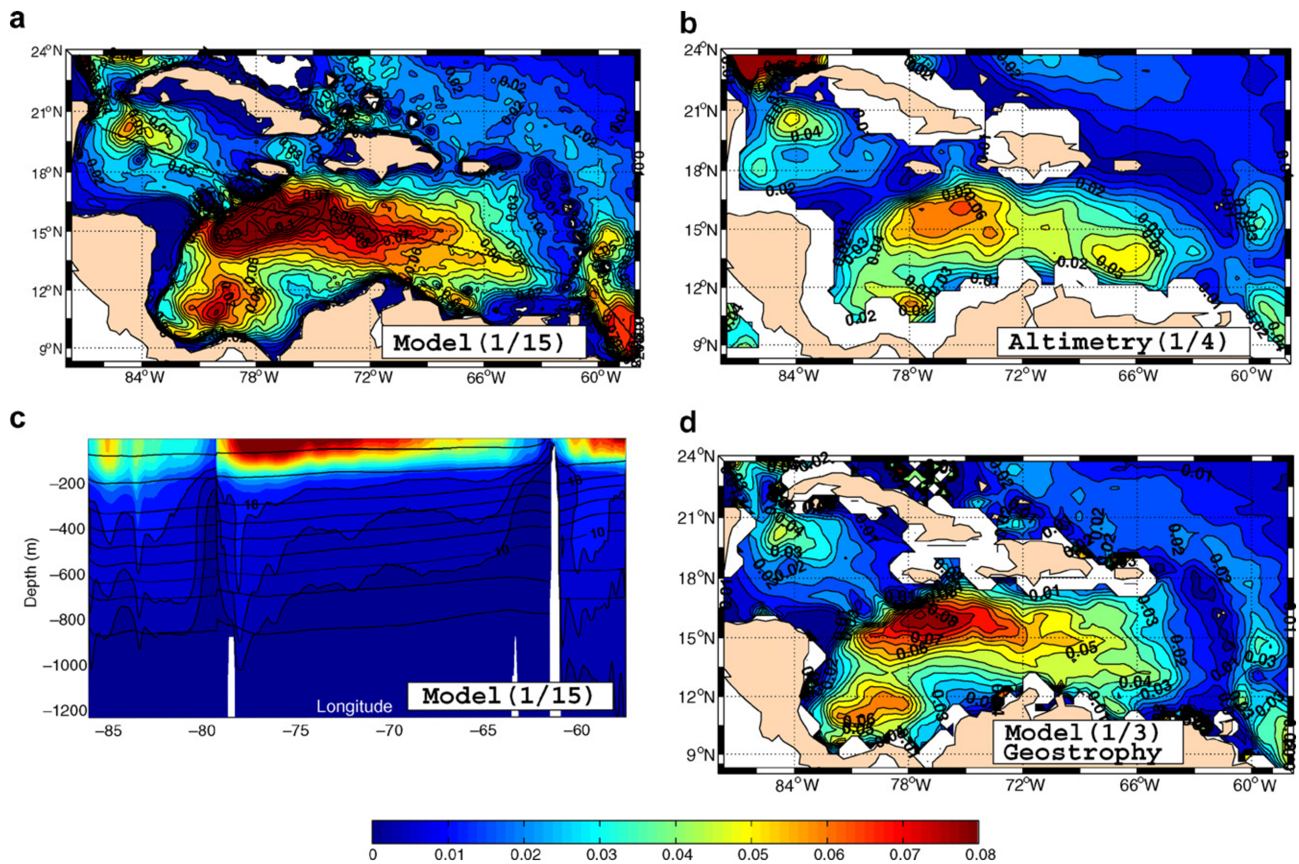

Fig. 13. (a) Model mean eddy kinetic energy (MEKE; $m^2\,s^{-2}$) calculated as a 6 years average of surface data from NOSLIP. Velocity anomalies are calculated subtracting the 6 years mean to the simulated data. (b) MEKE calculated with 5 years of geostrophic velocity anomalies. (c) Zonal section of MEKE for model data following the black line indicated in (a). (d) MEKE derived from 6 years of model geostrophic velocities, calculated using 5 days averages of coarse grid SSH from NOSLIP experiment. The color scale is the same between the different figures.

- MEKE of the NOSLIP experiment (Fig. 13a) gives some insights on the effect of the boundaries and more particularly of the Lesser Antilles. We compare it with the MEKE field from REF, displayed in Fig. 14b. In the NOSLIP experiment, the maximum of variability is moved westward near Jamaica and Nicaragua, perhaps due to the increased shear of currents near the coast which could generate more eddies or destabilize the large eddies which are traveling in the Colombia Basin. Outside the Caribbean, all along the Lesser Antilles chain, a band of variability is observed in NOSLIP but not in REF. In REF this incoming variability, associated with the NBC rings does not travel up to the Barbados Islands. In NOSLIP, some NBC rings travel further north and reach the Anageda Passage, at the northern limit of the Lesser Antilles. Movies made from model results show eddies entering the Caribbean Sea through this Passage. Eddies have been observed at 16°N (Rhein et al., 2005) and drifters show eddies up to 17°N (Richardson, 2005). In this respect results from NOSLIP are more realistic in reproducing the behavior of the incoming eddies near the Lesser Antilles.
- A local maximum of variability in the Panama–Colombia Gyre is only represented in the high resolution experiments: in CLIPPER and COARSE experiments, this region does not show high MEKE values. It indicates that the variability of the Panama–Colombia Gyre is resolution dependent. It will be seen in part II that the eastward flow is unstable, so such instability is better resolved by increasing the horizontal resolution.
- In VISC experiment, note how low values of MEKE occur east of the Lesser Antilles. These low values are due to the damping of all the Atlantic mesoscale variability near the Lesser Antilles in VISC. In contrast, the MEKE field inside the Caribbean Sea for this experiment remains energetic and of the same order of magnitude and horizontal distribution than in the other experiments. A natural question arises regarding the influence of the Atlantic variability on the Caribbean variability. It will be answered in part II by a more detailed comparison of this experiment with the other ones.

4.4. Complex EOF analysis

A complex empirical orthogonal function (CEOF; e.g., Barnett, 1983) analysis is used to isolate propagating structures in the Caribbean. The analysis is applied to the model SSH (NOSLIP experiment) and to the altimetry SSH (AVISO). The complex time series at each point are generated using a Hilbert transform of the SSH data for both model and observations. In both cases, the trend and annual cycle were previously removed. In Fig. 15, a snapshot of the real part of the reconstructed time series for mode 1, together with the corresponding variance conserving spectrum of real part of the time series, are displayed for each data set. The first EOF mode for model data and altimetry data account both for 20% of the variance. Both show a structure which propagates westward with peak periods centered at 75 days for altimetry data and 65 days for model data. Altimetry data also shows two additional peaks at 120 and 90 days. Depending on the time period over which the analysis is applied to altimetry data, the relative intensity of these peaks varies leading some peaks to be insignificant. It is indicative of a marked interannual variability of the frequency of the eddies, which the model cannot reproduce since climatological forcings are used. Such interannual variability is highlighted by

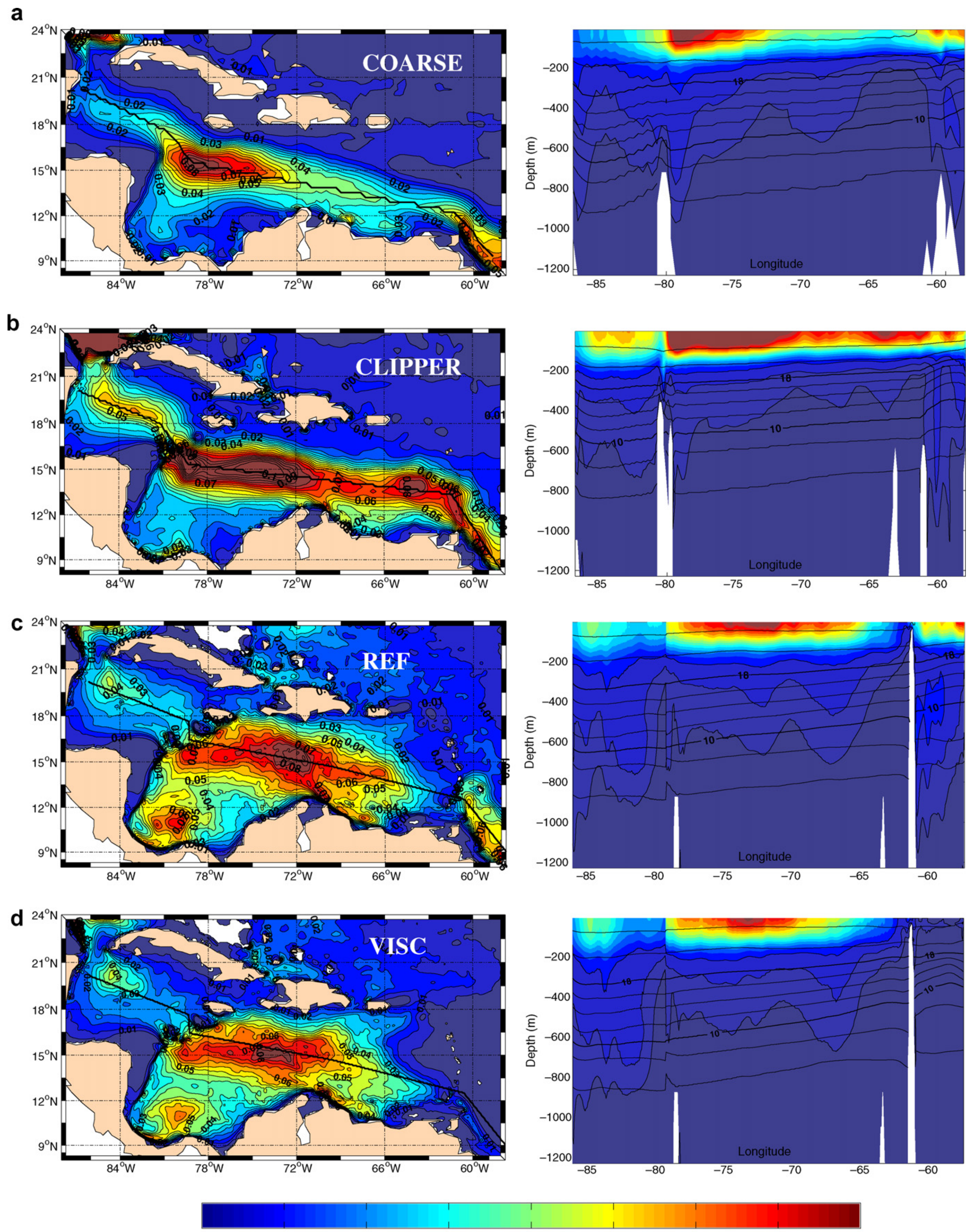

Fig. 14. Surface (left column) and zonal section (right column) of MEKE $m^2\,s^{-2}$ for experiments (a) COARSE (1/3°), (b) CLIPPER (1/6°), (c) REF (1/15°) and (d) VISC (1/15°). Velocity anomalies are calculated subtracting a 6 years mean average to the instantaneous velocity field. Sections were made along the corresponding black lines indicated on figures located on the left column.

Please cite this article in press as: Jouanno, J. et al., The mesoscale variability in the Caribbean Sea. Part I: Simulations ..., Ocean Modell. (2008), doi:10.1016/j.ocemod.2008.04.002

the temporal evolution of the phase (bottom in Fig. 15) which is much more regular in the model than in altimetry data.

Consistent with results of the precedent section, the first mode increases in amplitude and diameter from the Lesser Antilles to 75°W where it reaches its maximum in the Colombia Basin, with length scales up to 500 km width. The westward gain in amplitude is indicative of a westward strengthening of the eddies. The large Caribbean eddies influence the Panama–Colombia Gyre since it can be seen in both model and altimetry data that there is a large anomaly extending from the Colombia Basin to the Panama coast. In the Cayman Basin, patterns present less amplitude and smaller zonal wavelength. For both data sets, east of 70°W (i.e., in the Venezuela Basin) we can distinguish a northern and a southern band of variability (they are indicated by quasi-zonal dashed line in Fig. 15). These two bands merge near 70°W to give rise to larger patterns. First, it illustrates that most of the Caribbean mesoscale variability originates in the Eastern Caribbean Basin, in contrast to Oey et al. (2003) who proposed that most of the eddies form south of Hispaniola by the action of a strong Wind Stress Curl. Second, from a statistical point of view it confirms a behavior we have observed in animations from altimetry and model outputs: merging and interaction between eddies is an ubiquitous process which contributes to increase the size of the eddies. A careful look at maps of MEKE in Fig. 13, does not allow to distinguish a northern from a southern band of MEKE in the Venezuela Basin. The reason is an overlapping of the two bands. To gain some intuition about the existence of a northern band of variability in NOSLIP experiment, it is useful to compare model MEKE in Fig. 13 with model MEKE for COARSE or Clipper experiments in Fig. 14, for which high MEKE values are only seen in the southern Venezuela Basin, since these experiments do not produce eddies in the northern Venezuela Basin.

As shown in a previous section, the Caribbean flow is not a wide and homogeneous current; it does not advect all the eddies at the same speed. For example, an eddy embedded in the sCC in the Venezuela Basin will be advected westward at speeds up to 0.4 m s^{-1} whereas an eddy produced near the northern passages will travel at speeds of order 0.1 m s^{-1}. Such different speeds of advection should help interactions, collisions or merging among the eddies in comparison with a situation where all the structures would be advected at the same speed. Obviously, the growth of the perturbations also facilitates the merging between anticyclones since the probability that two structures interact increases with their diameter.

Finally, the agreement between model and altimeter results, suggests that the model captures the basic features of observed surface variability, even though it uses climatological seasonal forcing, which suggest that variability is controlled by internal dynamics rather than forced by external agents.

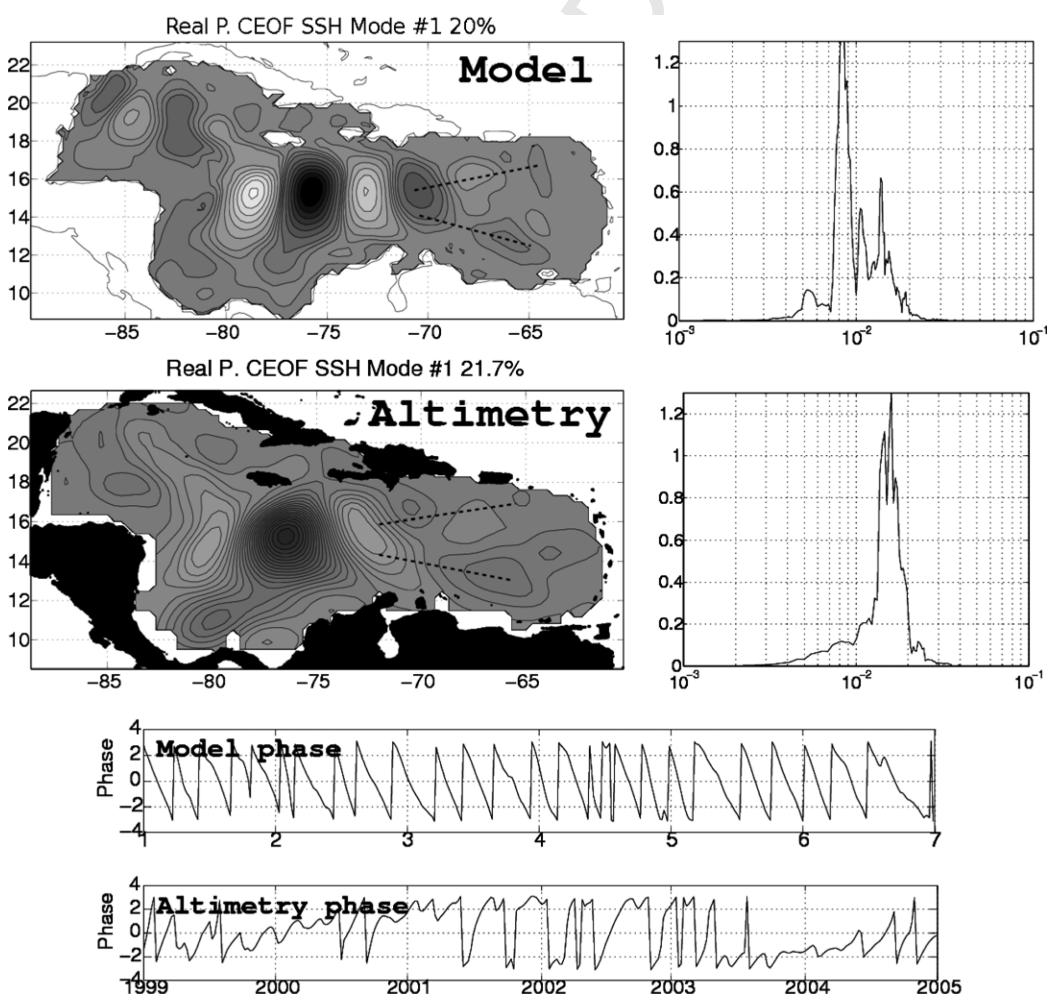

Fig. 15. First mode of the Complex EOF (CEOF) calculated with 6 years of model SSH (NOSLIP) and 12 years (1992–2004) of altimetry SSH. Variance conserving spectra (frequency in cycle/day vs. m^2 cycle/days) of the temporal evolution of the first mode and the corresponding temporal phase are also given. For model data, the first mode accounts for 20% of the variance, and for altimetry data it accounts for 21% of the variance. They illustrate the westward growth of the eddies and the agreement between model and altimetry results.

Please cite this article in press as: Jouanno, J. et al., The mesoscale variability in the Caribbean Sea. Part I: Simulations ..., Ocean Modell. (2008), doi:10.1016/j.ocemod.2008.04.002

4.5. Frequency of the mesoscale variability

In order to show the main frequencies of the variability and its zonal evolution, variance conserving spectra of model and altimetry SSH are computed for 4 meridional sections located in different regions, indicated in Fig. 10 with dashed line. The annual cycle was previously removed by fitting a sinusoidal to the SSH data sets. Comparing the different spectra calculated with model data (bold line in Fig. 16), we can see that the amplitude of the spectral peaks for periods higher than 100 days increases westward. This behavior is consistent with a westward increase of MEKE. A closer look shows that the more energetic band undergoes a westward shift toward higher periods: from 45–80 days in the Atlantic, to 50–90 days in Venezuela, to 60–80 days in Colombia and to 85–110 days in Cayman. This frequency shift along the Caribbean needs to be explained. First, the narrow channels between Jamaica and Nicaragua can act as filters allowing some eddies to trigger perturbations in Cayman Basin and others to be dissipated. Moreover, simulations show that the Jamaican Ridge can detains some eddies until they merge with a second to form a new larger eddy. This might explain the strong difference between the main peaks in "Cayman", of 85–110 days, and the peaks in the eastern basins of periods under 80 days. Between "Colombia" and "Venezuela", the slight frequency shift is a sign of the westward growth and merging of the disturbances, as discussed in the previous section.

Spectra calculated with altimetry data (thick line in Fig. 16) are in good agreement with spectra calculated with model data, and also show a westward shift toward lower frequencies. Among the differences, maybe the most important is the occurrence for altimetry data of a low frequency peak (160 days in "Atlantic" and around 120 days for the three other sections inside the Caribbean Basin). There is no trace of such peaks in model data. It is remarkable that these low frequency peaks in the Caribbean, which also appear in spectra calculated with geostrophic velocity anomalies derived from altimetry (not shown), are equal for the three Caribbean Basin sections and different for the "Atlantic" section. As for the CEOF analysis in Section 4.4, the occurrence of this peak depends on the period of data which is used. We are presently running interannual forcing experiment to investigate this. For the region "Atlantic", it can be clearly seen in Fig. 16 that the main peaks for altimetry spectra extend toward higher frequencies. Although in the figure the difference appears important, we consider it very low and not relevant: the main peaks range from 45 to 80 days for the model spectra and from 40 to 80 days for the altimeter spectra. In Colombia and Venezuela, the spectra for both data sets are in very good agreement. In Cayman we observe a slight difference of order 5 days between the main peaks of model and altimetry spectra, which is not significant since it is the period of data storage.

Finally, it is remarkable that the amplitude of the altimetry and model frequency peaks, which represents the energy associated to each frequency, are very close. Together with the close correspondence of the main frequency peaks, it confirms a pertinent representation of the mesoscale variability by the model. Another important result from this analysis is that the dominant frequency in the Cayman Sea, very close to the frequency of the events in the Yucatan Channel (not shown), is significantly different from the frequency of the events in the Colombia, Venezuela and Atlantic Basins. The connectivity between the different basins is not evident: even if there is an upstream influence on the downstream basin (Cayman), this influence does not set all the variability downstream. This could explain why Murphy et al. (1999) did not find any obvious connectivity between NBC rings and Loop Current eddy shedding.

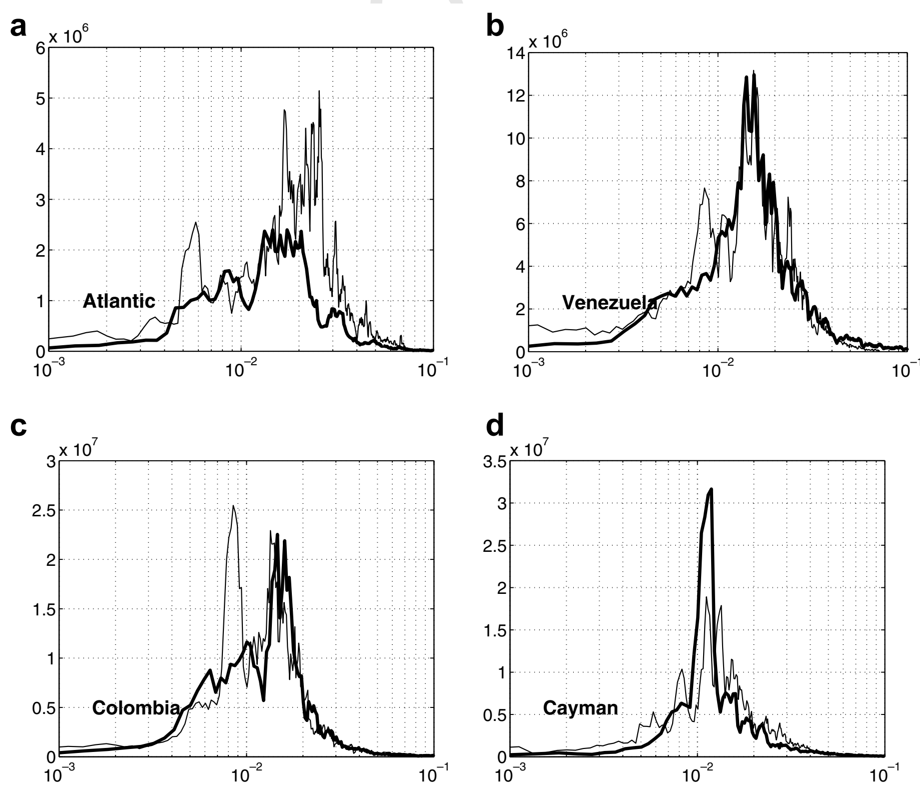

Fig. 16. Variance conserving spectrum (frequency in cycle/day vs. m^2 cycle/day) of SSH on four sections located respectively at (a) 57.4°W from 7.5°N to 15.4°N, (b) 69.3°W from 11.5°N to 18.6°N, (c) 78°W from 11°N to 18.7°N and (d) 85°W from 16.2°N to 21.9°N. These sections are indicated by four dashed meridional black lines in Fig. 10. Spectra are calculated with 6 years of model data (bold line) and 12 years of altimetry data (thick lines). Each spectrum plotted here is an average of the spectra at each point of the sections. Comparing the spectra, it can be seen a westward shift toward lower frequencies.

Please cite this article in press as: Jouanno, J. et al., The mesoscale variability in the Caribbean Sea. Part I: Simulations ..., Ocean Modell. (2008), doi:10.1016/j.ocemod.2008.04.002

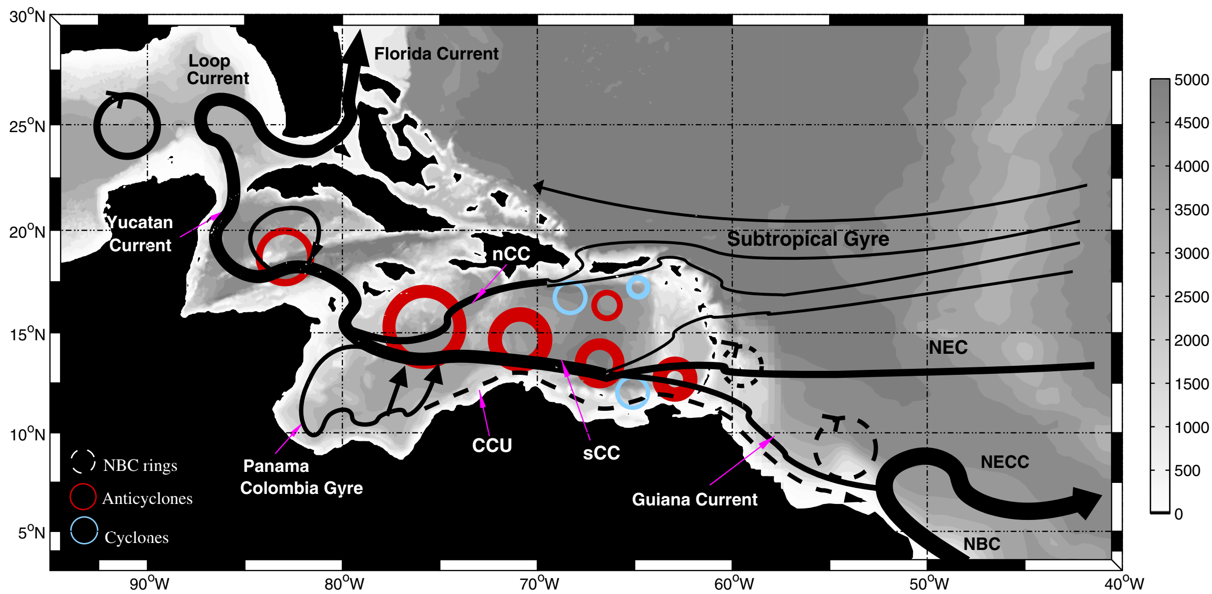

Fig. 17. Illustration of the main current paths inside and outside the Caribbean Sea: North Brazil Current (NBC), North Equatorial Current (NEC), southern Caribbean Current (sCC), northern Caribbean Current (nCC) and Caribbean Coastal Undercurrent (CCU). Circles represent structures moving westward: NBC rings (dashed), anticyclonic (red) and cyclonic (blue) Caribbean eddies. There is no clear indication that NBC rings can enter the Caribbean (e.g., Fratantoni and Richardson, 2006, part II of this study) as fully coherent structures. This is why we have chosen not represent their entrance. The gray scale is the bathymetry (m).

5. Summary and conclusions

The aim of this study was to provide a robust validation of the model and in parallel to present new findings on the Caribbean mean flow and eddy field.

Numerical experiments were carried out with a 2-way nested configuration of the NEMO model. Circulation in the Caribbean Sea and the Gulf of Mexico was simulated with a high resolution grid (1/15°) embedded in a coarser North Atlantic grid (1/3°). Comparisons between different numerical experiments allowed to show: (1) the robustness of some features which survive to changes of configuration; (2) the improvement brought by increasing resolution and the recent NEMO code vs. the former OPA code; and (3) the efficiency of using an embedded configuration in this region.

This study does not focus on describing the circulation produced by the North Atlantic grid, but it appears that the model reproduces the characteristic patterns of the North Atlantic circulation (rings from the North Brazil Current, Rossby waves, variability of the MOC and Subtropical Gyre) which are important due to their interaction with the Caribbean circulation. In the Caribbean, the 1/15° “child” grid allows a fine representation of geography and bottom topography of the Antilles Chain, and also an adequate resolution of instability processes.

A sketch of the main current paths is drawn in Fig. 17, to illustrate the comments that follow. The Caribbean inflow, formed with waters from the Subtropical Gyre and the MOC, is shown to organize into two zonal jets, the sCC (intense, strong vertical shear) and the nCC (low, deep), flowing westward respectively along the southern and northern boundaries of the Venezuela Basin, which then merge in the center of the Colombia Basin. Some regions present local velocity maxima and particularly strong vertical and horizontal shear which will be linked in part II with eddy production. The vertical extent of the main mean current core reaches 200 m depth in the Colombia and Venezuela Basin and more than 700 m depth in the Cayman Basin.

The largest simulated Caribbean eddies are anticyclones which travel westward with a speed ranging between 12 and 15 cm s^{-1}, whose width ranges between 200 and 500 km and have time scales between 50 and 110 days. Vertically, their core is generally limited to 200 m depth, but velocity anomalies can reach depths down to 1000 m. For all the experiments, the eddy kinetic energy increases and deepen westward in the Colombia/Venezuela Basins, associated with a westward strengthening of the eddies as illustrated in Fig. 17. In contrast to the variability in these basins, the variability in the Cayman Basin is less energetic, deeper and of lower frequency. The connectivity between the different basins is not evident: even if there is an upstream influence of the Colombia Basin on the downstream basin (Cayman), this influence does not set all the characteristics of the variability downstream.

The westward growth of the eddies observed in Colombia/Venezuela Basin but also in Cayman Basin comes to suggest that there are energy sources for the mesoscale variability which are internal to the Caribbean region. This point is addressed in part II (Jouanno et al., submitted).

Acknowledgments

We acknowledge the provision of supercomputing facilities by the Institut pour le Développement des Ressources en Informantique Scientifique of the Centre National de la Recherche Scientifique, by the Departamento de Supercomputo of the UNAM and by the CICESE (Conacyt Project SEP-2003-C02-44534). Some computations were also performed at Bakliz of DGSCA, UNAM. The altimeter products were produced by the CLS Space Oceanography Division as part of the Environment and Climate EU ENACT Project (EVK2-CT2001-00117) and with support of the CNES. Geostrophic velocity anomalies were produced by Ssalto/Duacs and distributed by Aviso, with support from Cnes. The fine grid/coarse grid model configuration was set up in a cooperation between CICESE and the Drakkar Project (www.ifremer.fr/lpo/drakkar).

References

Abascal, A.J., Sheinbaum, J., Candela, J., Ochoa, J., Badan, A., 2003. Analysis of flow variability in the Yucatan Channel. J. Geophys. Res. 108 (C12), 3381.

Andrade, C.A., Barton, E.D., 2000. Eddy development and motion in the Caribbean Sea. J. Geophys. Res. 105 (C11), 26191–26201.

Andrade, C.B., Barton, E.D., Mooers, C.N.K., 2003. Evidence for an eastward flow along the Central and South American Caribbean Coast. J. Geophys. Res. 108 (C6), 3185. doi:10.1029/2002JC001549.

Barnett, T.P., 1983. Interaction of the monsoon and Pacific trade wind system at interannual time scale: Part 1. Mon. Weather Rev. 111, 756–773.

Barnier, B., 1998. Forcing the Ocean. In: Chassignet, E.P., Verron, J. (Eds.), Ocean Modeling and Parameterization. Kluwer Academic Publishers, The Netherlands, pp. 45–80.

Barnier, B., Madec, G., Penduff, T., Molines, J., Treguier, A., Sommer, J.L., Beckmann, A., Biastoch, A., Böning, C., Dengg, J., Derval, C., Durand, E., Gulev, S., Remy, E., Talandier, C., Theeten, S., Maltrud, M., McClean, J., Cuevas, B.D., 2006. Impact of partial steps and momentum advection schemes in a global ocean circulation model at eddy-permitting resolution. Ocean Dyn.. doi:10.1007/S10236-006-0082-1.

Barnier, S., Reynaud, T., Beckman, A., Boning, C., Molines, J.M., Bernard, S., Jia, Y., 2001. On the seasonal variability and eddies in the North Brazil Current: insights from model inter-comparison experiments. Progr. Oceanogr. 48, 195–230.

Blanke, B., Delecluse, P., 1993. Variability of the tropical Atlantic ocean simulated by a general circulation model with two different mixed-layer physics. J. Phys. Oceanogr. 23, 1363–1388.

Blayo, E., Debreu, L., 1999. Adaptive mesh refinement for finite-difference ocean models: first experiments. J. Phys. Oceanogr. 32, 1239–1250.

Cailleau, S., 2004. Validation de méthodes de contrainte aux frontières d'un modèle océanique: application à un modèle hauturier de l'Atlantique Nord et à un modèle régional du Golfe de Gascogne. Ph.D. Thesis, Université Joseph Fourier, Grenoble, France.

Cailleau, S., Fedorenko, V., Barnier, B., Blayo, E., Debreu, L., accepted for publication. Comparison of different numerical methods used to handle the open boundary Q1 of a regional ocean circulation model of the Bay of Biscay. Ocean Modell..

Candela, J., Tanahara, S., Crepon, M., Barnier, B., Sheinbaum, J., 2003. Yucatan Channel flow: observations versus CLIPPER ATL6 and MERCATOR PAM models. J. Geophys. Res. 108 (C12), 3385. doi:10.1029/2003JC001961.

Carton, J.A., Chao, Y., 1999. Caribbean Sea eddies inferred from TOPEX/Poseidon altimetry and a 1/6 Atlantic ocean model circulation. J. Geophys. Res. 104 (C4), 7743–7752.

Centurioni, L.R., Niiler, P.P., 2003. On the surface currents of the Caribbean Sea. Geophys. Res. Lett. 30 (6), 1279. doi:10.1029/2002GL016231.

Chanut, J., 2003. Paramétrisation de la restratification après convection profonde en Mer du Labrador. Ph.D. Thesis, Université Joseph Fourier, Grenoble, France.

Chanut, J., Barnier, B., Large, W., Debreu, L., Penduff, T., Molines, J., Mathiot, P., in press. Mesoscale eddies in the Labrador Sea and their contribution to Q2 convection and re-stratification. J. Phys. Oceanogr..

Debreu, L., 2000. Raffinement adaptatif de maillage et méthode de zoom. Application aux modeles d'océan. Ph.D. Thesis, Université Joseph Fourier, Grenoble, France.

Debreu, L., Blayo, E., Barnier, B., 2005. A general multi-resolution approach to ocean modelling: experiments in a primitive equation model of the north Atlantic. In: Tomasz, P., Timur, L., Gregory Weirs, V., (Eds.), Adaptive Mesh Refinement – Theory and Applications, Lecture Notes in Computer Science, vol. 41.

Fratantoni, D.M., Richardson, P.L., 2006. The evolution and demise of North Brazil Current rings. J. Phys. Oceanogr. 36, 1241–1264.

Garnier, E., Barnier, B., Siefridt, L., Beranger, K., 2001. Investigating the 15-year air sea flux climatology from ECMWF re-analysis project as a surface boundary condition for ocean models. Int. J. Climatol. 20, 1653–1673.

Group, T.R., 1981. Gulf stream cold-core rings: their physics, chemistry, and biology. Science 212, 1091–1100.

Guerrero, L., Sheinbaum, J., Candela, J., in preparation. Surface variability and the Q3 tracking of eddies in the caribbean sea.

Hernández-Guerra, Joyce, T., 2000. Water masses and circulation in the surface layers of the Caribbean at 66°W. Geophys. Res. Lett. 27, 3497–3500.

IOC, I., BODC, 2003. Centenary Edition of the GEBCO Digital Atlas, published on CD-ROM on behalf of the intergovernmental Oceanographic Commission and the International Hydrographic Organization as part of the General Bathymetric Chart of the Oceans. Technical report, British Oceanographic Data Centre, Liverpool, UK.

Johns, W., 2007. Dynamics of boundary currents and marginal seas: windward passage experiment. Technical report, University of Miami, RSMAS/MPO.

Johns, W.E., Townsend, T.L., Fratantoni, D.M., Wilson, W.D., 2002. On the Atlantic inflow to the Caribbean Sea. Deep Sea Res. I 49, 211–243.

Johns, W.E., Zantopp, R.J., Goni, G.J., 2003. Cross-gyre transport by North Brazil Current rings. In: Goni, G.J., Malanotte-Rizzoli, P. (Eds.), Interhemispheric Water Exchange in the Atlantic Ocean. Elsevier Oceanographic Series, vol. 68, pp. 411–441.

Jouanno, J., Sheinbaum, J., Barnier, B., Molines, J.M., submitted. The mesoscale variability in the caribbean sea. part II: energy sources. Ocean Modeling. Q4

Larsen, J., 1992. Transport and heat flux of the Florida Current at 27 °n derived from cross-stream voltages and profiling data: theory and observations. Philos. Trans. Roy. Soc. Lond. A 338, 169–236.

Leeman, K.D., Vertes, P., Atkinson, L., Lee, T., Hamilton, P., Waddell, E., 1995. Transport, potential vorticity, and current/temperature structure across North West Providence and Santaren channels and the Florida Current off Cay Sal Bank. J. Geophys. Res. 100, 8561–8569.

Madec, G., Delecluse, P., Imbard, M., Lévy, C., 1998. Opa 8.1 Ocean general circulation model reference manual. Institut Pierre-Simmon Laplace, vol. 20, p. 91.

Murphy, S.J., Hurlburt, H.E., O'Brien, J.J., 1999. The connectivity of eddy variability in the Caribbean Sea the Gulf of Mexico and the Atlantic Ocean. J. Geophys. Res. 94 (C1), 1431–1453.

Niiler, P., Maximenko, N., McWilliams, J., 2003. Dynamically balanced absolute sea level of the global ocean derived from near-surface velocity observations. Geophys. Res. Lett. 30 (22). doi:10.1029/2003GL018628.

Niiler, P.P., Richardson, P.L., 1973. Seasonal variability of the Florida Current. J. Mar. Res. 31, 144–167.

Oey, L.-Y., Lee, H.-C., Schmitz Jr., W.J., 2003. Effect of winds and Caribbean eddies on the frequency of Loop Current eddy shedding: a numerical model study. J. Geophys. Res. 108 (C10), 3324. doi:10.1029/2002JC001698.

Penduff, T., Barnier, B., Dewar, W., O'Brien, J., 2004. Dynamical response to the oceanic eddy field to the North Atlantic Oscillation: a model-data comparison. J. Phys. Oceanogr. 34, 2615–2629.

Penduff, T., Sommer, J.L., Barnier, B., Treguier, A., Molines, J., Madec, G., 2007. Influence of numerical schemes on current-topography interactions in 1/4° global ocean simulations. Ocean Sci. 3, 1–16.

Penven, P., Debreu, L., Marchesiello, P., McWilliams, J.C., 2006. Evaluation and application of the ROMS 1-way embedding procedure to the central california upwelling system. Ocean Modell. 12, 157–187.

Reynaud, T., Legrand, P., Mercier, H., Barnier, B., 1998. A new analysis of hydrographic data in the Atlantic and its application to an inverse modeling study. Int. WOCE Newslett. 32, 29–31.

Rhein, M., Kirchner, K., Mertens, C., Steinfeldt, R., Walter, M., Fleischmann-Wischnath, U., 2005. Transport of South Atlantic Water through the passages south of Guadeloupe and across 16°N, 2000–2004. Deep Sea Res. I 52 (12), 2234–2249.

Richardson, P., 2005. Caribbean Current and eddies as observed by surface drifters. Deep Sea Res. II 52, 429–463.

Sadoumy, R., 1975. The dynamics of finite difference models of the shallow-water equations. J. Atmos. Sci. 32 (4), 680–689.

Schmitz, W.J.J., McCartney, M.S., 1993. On the North Atlantic circulation. Rev. Geophys. 31, 29–44.

Sheinbaum, J., Candela, J., Badán, A., Ochoa, J., 2002. Flow structure and transport in Yucatan channel. Geophys. Res. Lett. 29 (3), 1040. doi:10.1029/2001GL013990.

Silander, M., 2005. On the Three-Dimensional Structure of Caribbean Mesoscale Eddies. Thesis of the University of Puerto Rico.

Smith, R., Johns, W., Johns, E., 2007. Volume transport and variability at Windward Passage. EOS Trans. AGU, Jt. Assem. Suppl. 88 (23) (Abstract OS52A-08).

Smith, W.H.F., Sandwell, D.T., 1997. Global seafloor topography from satellite altimetry and ship depth soundings. Science 277, 1957–1962.

Talley, L.D., Reid, J., Robbins, P., 2003. Data-based meridional overturning streamfunctions for the global oceans. J. Climate 16, 3213–3226.

Tanahara, S., 2004. Etude de la circulation dans le Golfe du Mexique et la Mer des Caraibes. Validation des simulations CLIPPER-ATL6 a l'aide des observations CANEK. Thèse de l'Université Pierre et Marie Curie – Paris6.

Tréguier, A.M., Reynaud, T., Pichevin, T., Barnier, B., Molines, J., de Miranda, A., Messager, C., Beismann, J., Madec, G., Grima, N., Imbard, M., Provost, C.L., 1999. The CLIPPER project: high resolution modeling of the Atlantic. Int. WOCE Newslett. 36, 3–5.

Tréguier, A.M., Barnier, B., de Miranda, A., Molines, J., Grima, N., Imbard, M., Madec, G., Messager, C., Michel, S., 2001. An eddy permitting model of the Atlantic circulation: evaluating open boundary conditions. J. Geophys. Res. 106 (C10), 22,115–22,130.